Cancer Cell

Article

Genome-wide CRISPR screens of T cell exhaustion identify chromatin remodeling factors that limit T cell persistence

Graphical abstract

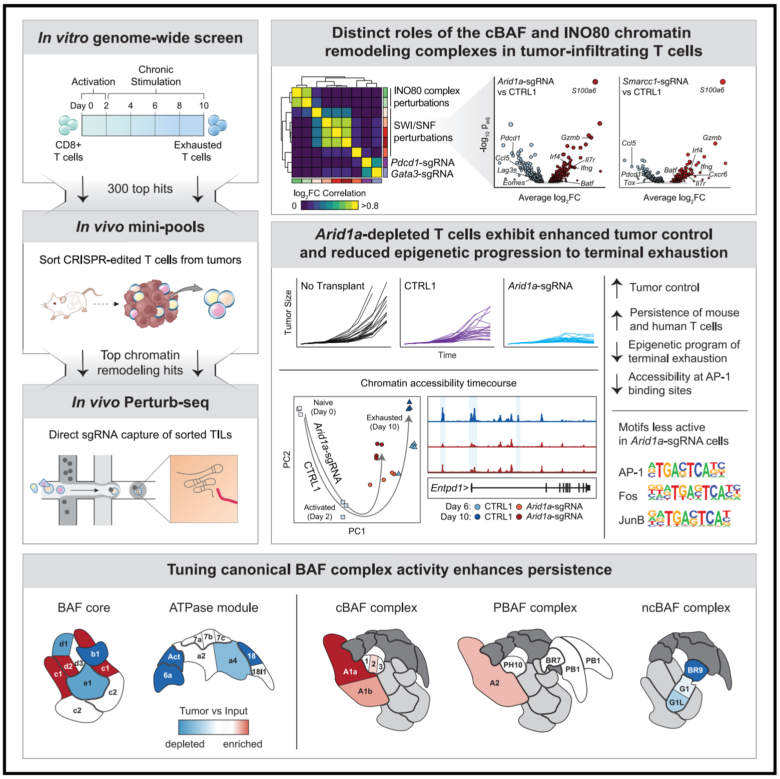

Highlights

- *In vitro* T cell exhaustion assay enables genome-wide CRISPR-Cas9 screening
- *In vitro* and *in vivo* genetic screens converge on cBAF and INO80 complex subunits
- *Arid1a*-sgRNA T cells improve tumor control and enhance persistence of human T cells
- *Arid1a* is required for acquisition of the epigenetic state of terminal exhaustion

Authors

Julia A. Belk, Winnie Yao, Nghi Ly, ..., Julia Carnevale, Santosh A. Vardhana, Ansuman T. Satpathy

Correspondence

satpathy@stanford.edu

In brief

Belk et al. systematically dissect the genetic regulators of T cell exhaustion with a series of *in vitro* and *in vivo* CRISPR-Cas9 screens. The depletion of chromatin remodeling factors, in particular *Arid1a*, improves T cell function and reduces the transcriptional and epigenetic hallmarks of exhaustion.

Belk et al., 2022, Cancer Cell *40*, 1–19
July 11, 2022
https://doi.org/10.1016/j.ccell.2022.06.001

CellPress

Please cite this article in press as: Belk et al., Genome-wide CRISPR screens of T cell exhaustion identify chromatin remodeling factors that limit T cell persistence, Cancer Cell (2022), https://doi.org/10.1016/j.ccell.2022.06.001

Cancer Cell

CellPress

Article

Genome-wide CRISPR screens of T cell exhaustion identify chromatin remodeling factors that limit T cell persistence

Julia A. Belk,[1,2] Winnie Yao,[3] Nghi Ly,[3] Katherine A. Freitas,[4,5] Yan-Ting Chen,[6] Quanming Shi,[3] Alfredo M. Valencia,[7,8] Eric Shifrut,[2] Nupura Kale,[9] Kathryn E. Yost,[10] Connor V. Duffy,[11] Bence Daniel,[2,3] Madeline A. Hwee,[6] Zhuang Miao,[11] Alan Ashworth,[9,12] Crystal L. Mackall,[13,14,15,16] Alexander Marson,[2,9,12,13,17,18,19] Julia Carnevale,[2,9] Santosh A. Vardhana,[6,13] and Ansuman T. Satpathy[2,3,4,13,16,20,*]

[1]Department of Computer Science, Stanford University, Stanford, CA 94305, USA
[2]Gladstone-UCSF Institute of Genomic Immunology, San Francisco, CA 94158, USA
[3]Department of Pathology, Stanford University, Stanford, CA 94305, USA
[4]Immunology Graduate Program, Stanford University School of Medicine, Stanford, CA 94035, USA
[5]Center for Cancer Cell Therapy, Stanford Cancer Institute, Stanford University School of Medicine, Stanford, CA 94035, USA
[6]Memorial Sloan Kettering Cancer Center, New York, NY, USA
[7]Department of Psychiatry and Behavioral Sciences, Stanford University, Stanford, CA 94305, USA
[8]Stanford Brain Organogenesis, Wu Tsai Neurosciences Institute, Stanford University, Stanford, CA 94305, USA
[9]UCSF Helen Diller Family Comprehensive Cancer Center, University of California, San Francisco, San Francisco, CA 94158, USA
[10]Cancer Biology Program, Stanford University School of Medicine, Stanford, CA, USA
[11]Department of Genetics, Stanford University, Stanford, CA 94305, USA
[12]Department of Medicine, University of California, San Francisco, San Francisco, CA 94143, USA
[13]Parker Institute of Cancer Immunotherapy, San Francisco, CA 94305, USA
[14]Division of Pediatric Hematology/Oncology/Stem Cell Transplant and Regenerative Medicine, Department of Pediatrics, Stanford University School of Medicine, Stanford, CA 94035, USA
[15]Division of BMT and Cell Therapy, Department of Medicine, Stanford University School of Medicine, Stanford, CA 94035, USA
[16]Stanford Cancer Institute, Stanford University School of Medicine, Stanford, CA 94305, USA
[17]Department of Microbiology and Immunology, University of California, San Francisco, San Francisco, CA 94143, USA
[18]Chan Zuckerberg Biohub, San Francisco, CA 94158, USA
[19]Innovative Genomics Institute, University of California, Berkeley, Berkeley, CA 94720, USA
[20]Lead contact
*Correspondence: satpathy@stanford.edu

https://doi.org/10.1016/j.ccell.2022.06.001

SUMMARY

T cell exhaustion limits antitumor immunity, but the molecular determinants of this process remain poorly understood. Using a chronic stimulation assay, we performed genome-wide CRISPR-Cas9 screens to systematically discover regulators of T cell exhaustion, which identified an enrichment of epigenetic factors. *In vivo* CRISPR screens in murine and human tumor models demonstrated that perturbation of the INO80 and BAF chromatin remodeling complexes improved T cell persistence in tumors. *In vivo* Perturb-seq revealed distinct transcriptional roles of each complex and that depletion of canonical BAF complex members, including *Arid1a*, resulted in the maintenance of an effector program and downregulation of exhaustion-related genes in tumor-infiltrating T cells. Finally, *Arid1a* depletion limited the acquisition of exhaustion-associated chromatin accessibility and led to improved antitumor immunity. In summary, we provide an atlas of the genetic regulators of T cell exhaustion and demonstrate that modulation of epigenetic state can improve T cell responses in cancer immunotherapy.

INTRODUCTION

T cell exhaustion is a process that is driven by chronic T cell receptor (TCR) stimulation and induces the stable expression of inhibitory surface receptors, poor response to tumor antigens, and low cell proliferation and persistence *in vivo* (Wherry and Kurachi, 2015; Collier et al., 2021). Originally identified in the setting of chronic viral infection (Zajac et al., 1998; Barber et al., 2006), T cell exhaustion is now appreciated to occur in diverse disease settings, including cancer and autoimmune disease (McKinney et al., 2015; McLane et al., 2019). Importantly, studies have demonstrated that T cell exhaustion represents a major barrier for the efficacy of both checkpoint blockade and chimeric antigen receptor T (CAR-T) cell immunotherapies, and

Please cite this article in press as: Belk et al., Genome-wide CRISPR screens of T cell exhaustion identify chromatin remodeling factors that limit T cell persistence, Cancer Cell (2022), https://doi.org/10.1016/j.ccell.2022.06.001

that manipulating this process may lead to the improved efficacy of T cell responses in cancer (Sakuishi et al., 2010; Long et al., 2015; Fraietta et al., 2018a, 2018b; Ribas and Wolchok, 2018; Lynn et al., 2019; Yost et al., 2019; Weber et al., 2021).

Recent genomic studies in murine models of chronic infection and cancer have demonstrated that T cell exhaustion is associated with a broad remodeling of the transcriptional and epigenomic landscape, which is conserved across disease settings (Pauken et al., 2016; Sen et al., 2016; Philip et al., 2017; Scott-Browne et al., 2016; Pritykin et al., 2021). This unique epigenetic state is primarily driven by chronic antigen and TCR signaling, and results in a stable cellular phenotype that is not changed by anti-programmed cell death protein 1 (PD-1) treatment (Pauken et al., 2016; Pritykin et al., 2021; Schietinger et al., 2016; Belk et al., 2022). Indeed, in cancer patients receiving PD-1 blockade, exhausted T cells display a distinct differentiation trajectory and end-stage chromatin profile, compared to functional effector T cells, and clonal tracing of exhausted T cells demonstrated that these cells are limited in their capacity to proliferate and perform effector functions in response to immunotherapy (Yost et al., 2019; Philip et al., 2017; Satpathy et al., 2019).

CRISPR-Cas9 screening has emerged as a powerful discovery tool for the molecular determinants of immune cell differentiation and function (Parnas et al., 2015; Shalem et al., 2014; Shifrut et al., 2018; Wang et al., 2014). For example, prior CRISPR-Cas9 screens in T cells have been used to identify transcription factors and metabolic regulators of T cell fate *in vivo*, as well as therapeutic targets (Chen et al., 2021; Dong et al., 2019; Huang et al., 2021; LaFleur et al., 2019; Wei et al., 2019). However, inherent limitations in scaling these *in vivo* assays have constrained library diversity of these screens, largely preventing genome-wide analysis and an unbiased discovery of novel regulators of T cell phenotypes. Furthermore, assays that simultaneously screen for multiple functions of T cells—for example, tissue localization, infiltration, and differentiation in tumors—have also made it challenging to interrogate the impact of a particular gene perturbation on a single aspect of T cell function and phenotype, such as exhaustion.

Here, we developed an *in vitro* model of CD8$^+$ T cell exhaustion, which recapitulates the epigenomic features of exhaustion that are observed *in vivo* and is scalable for genome-wide CRISPR-Cas9 screens. Using this model, we provide a comprehensive view of the genetic regulators of T cell exhaustion. Strikingly, these factors are enriched for chromatin remodeling proteins, including subunits of the INO80 (inositol requiring mutant 80) nucleosome positioning complex and the SWI/SNF (switch/sucrose non-fermentable) chromatin remodeling complex. Depletion of INO80 and canonical BRG1 or BRM-associated factor (cBAF; SWI/SNF family) complex members—in particular, *Arid1a*—led to increased persistence of T cells *in vivo*, and Perturb sequencing (Perturb-seq) analysis revealed distinct transcriptional programs controlled by each complex in tumor-infiltrating T cells. Epigenomic profiling of *Arid1a*-depleted T cells demonstrated that *Arid1a* was required for the acquisition of exhaustion-associated chromatin remodeling that occurs during chronic antigen stimulation. Finally, *Arid1a*-depleted cells exhibited improved tumor control, suggesting that the modulation of the epigenetic state of T cell exhaustion via chromatin remodeling factors may be an effective path to improve T cell responses in cancer immunotherapy.

RESULTS

An *in vitro* chronic stimulation assay recapitulates the epigenetic program of terminal T cell exhaustion

To develop an assay that is amenable to genome-wide CRISPR-Cas9 screening of T cell exhaustion, we adapted our previously described approach, which used anti-CD3 antibodies to enforce clustering of the T cell co-receptor, CD3, and thereby induce chronic TCR signaling in an antigen-independent manner (Figure 1A) (Vardhana et al., 2020). Compared to *in vivo* assays, this model isolates the core determinant of T cell exhaustion—chronic stimulation through the TCR complex—and removes T cell localization and trafficking effects, as well as immunosuppressive factors in the tumor microenvironment (TME). Importantly, this assay is scalable; we were able to culture upwards of 10^8 cells, enabling coverage of genome-wide CRISPR single-guide RNA (sgRNA) libraries. Over the course of 8 days of anti-CD3 stimulation (after 2 days of anti-CD3/CD28 activation), we confirmed a progressive upregulation of the inhibitory receptors, PD-1 and T cell immunoglobulin domain and mucin domain 3 (TIM3), and a growth defect in the chronically stimulated T cells, compared to cells passaged without further TCR stimulation after initial activation (acute stimulation; $p < 0.0001$, unpaired t test; Figures 1B, 1C, and S1A). Chronically stimulated T cells exhibited defects in the secretion of interferon γ (IFN-γ) and tumor necrosis factor α (TNF-α) after re-stimulation with phorbol myristate acetate and ionomycin (PMA/IO), compared to acutely stimulated cells, and defects in tumor killing *in vitro* and *in vivo* (Figures S1B–S1D).

We next asked whether the *in vitro* exhaustion assay recapitulated epigenetic hallmarks of T cell exhaustion *in vivo* (Pauken et al., 2016; Sen et al., 2016; Satpathy et al., 2019). We performed the assay for transposase-accessible chromatin with sequencing (ATAC-seq) over the course of chronic stimulation and analyzed chromatin accessibility profiles. Principal-component analysis (PCA) of ATAC-seq profiles showed that PC1 separated naive cells (day 0) from all of the other samples, while PC2 captured a progressive epigenetic differentiation of the T cells during chronic stimulation (Figure 1D). Analysis of individual gene loci, including *Pdcd1* and *Entpd1*, demonstrated an increase in accessibility at known exhaustion-specific regulatory elements (Figure 1E) (Miller et al., 2019). We evaluated the global epigenetic similarity of *in vitro* stimulated cells to reference T cell exhaustion data from tumors and chronic infection (Miller et al., 2019). We defined a terminal exhausted T cell (T_{EX}) peak set as ATAC-seq peaks that are specifically active in terminally exhausted T cells, compared to progenitor exhausted T cells, and we identified 3,537 terminal exhaustion ATAC-seq peaks in the B16 melanoma tumor model and 2,346 peaks in the lymphocytic choriomeningitis virus (LCMV) chronic infection model ($\log_2$ fold change [LFC] ≥ 1; FDR ≤ 0.05; Figures 1F and S1E–S1G). The *in vitro* assay recapitulated global epigenomic changes observed in terminal T_{EX} cells *in vivo* in both systems: 88.6% of ATAC-seq peaks in tumors and 70.1% of ATAC-seq peaks in chronic infection showed a shared increase in accessibility in the *in vitro* model at day 10 (false discovery rate

Please cite this article in press as: Belk et al., Genome-wide CRISPR screens of T cell exhaustion identify chromatin remodeling factors that limit T cell persistence, Cancer Cell (2022), https://doi.org/10.1016/j.ccell.2022.06.001

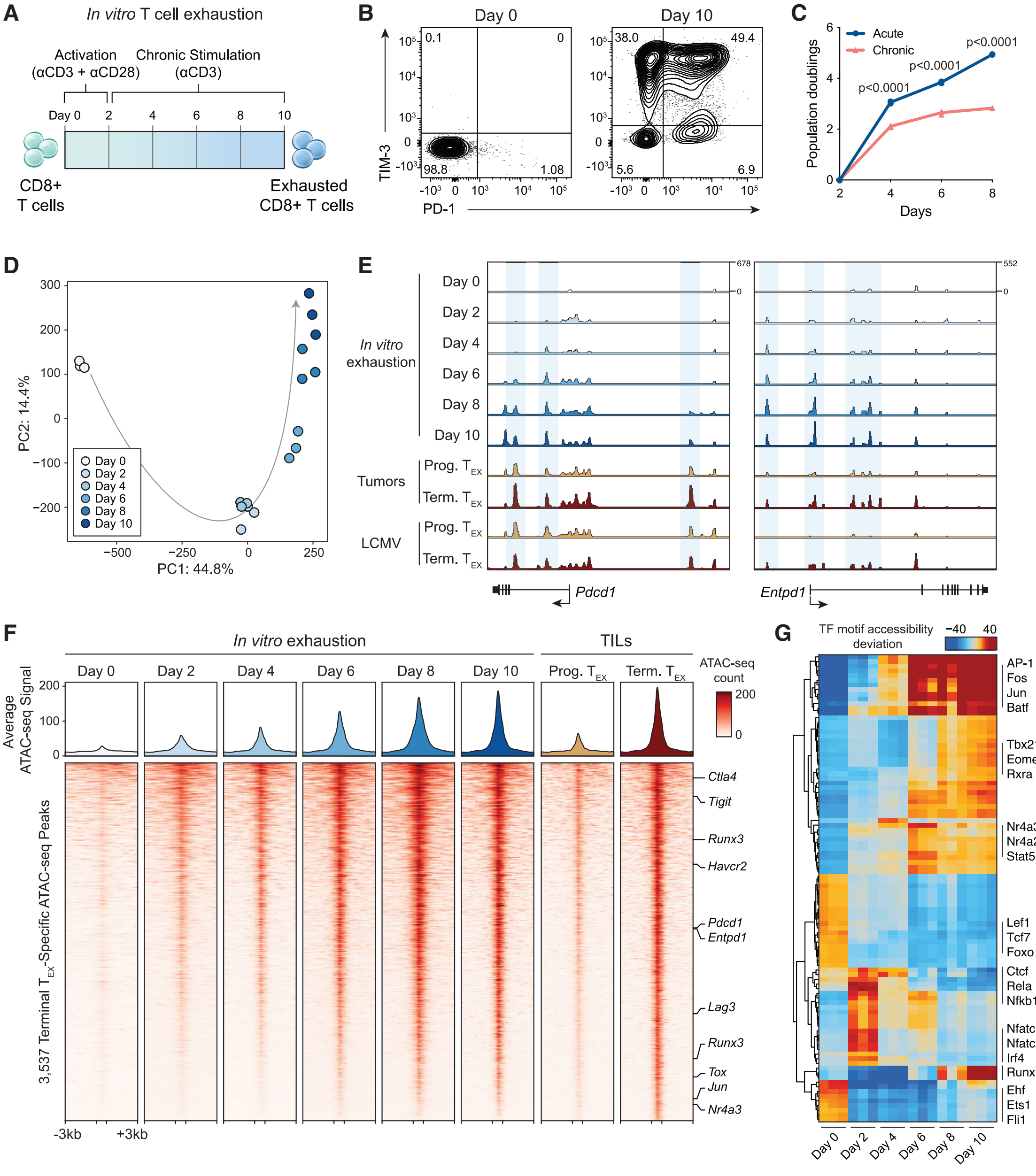

Figure 1. *In vitro* chronic antigen stimulation assay recapitulates the epigenetic hallmarks of T cell exhaustion

(A) Diagram of the *in vitro* exhaustion assay.

(B) Surface phenotype of $CD8^+$ T cells at days 0 and 10 of the T cell exhaustion assay, gated on live cells.

(C) Expansion of chronically stimulated and acutely stimulated T cells *in vitro*. Statistical significance was assessed by Student's t test, n = 3.

(D) Principal-component analysis of ATAC-seq profiles of $CD8^+$ T cells throughout the course of chronic stimulation, n = 3.

(E) ATAC-seq signal tracks in the *Pdcd1* and *Entpd1* gene loci at each time point in the *in vitro* exhaustion assay, as well as previously published reference ATAC-seq profiles from T cells in tumors or LCMV (Miller et al., 2019).

(F) Heatmap showing ATAC-seq coverage of each peak in the "terminal exhaustion peak set" for each time point in the *in vitro* exhaustion assay. Reference data from TILs is also included. Selected nearest genes are indicated on the right.

(G) chromVAR motif accessibility heatmap for each ATAC-seq sample. Selected TF motifs are indicated on the right. Top 100 most variable motifs are shown. See also Figure S1.

[FDR] $\leq$ 0.05; Figures 1F, S1F, and S1G). By contrast, analysis of the 2,926 progenitor T_{EX} peaks identified in tumor-infiltrating lymphocytes (TILs) demonstrated that these sites showed decreased accessibility with repeated stimulation (Figures S1E–S1G). Finally, we analyzed chromatin accessibility at transcription factor (TF) binding sites using chromVAR (Schep et al., 2017), which showed that TF motifs previously associated with terminal exhaustion, including Batf, Fos, Jun, and Nr4a

Please cite this article in press as: Belk et al., Genome-wide CRISPR screens of T cell exhaustion identify chromatin remodeling factors that limit T cell persistence, Cancer Cell (2022), https://doi.org/10.1016/j.ccell.2022.06.001

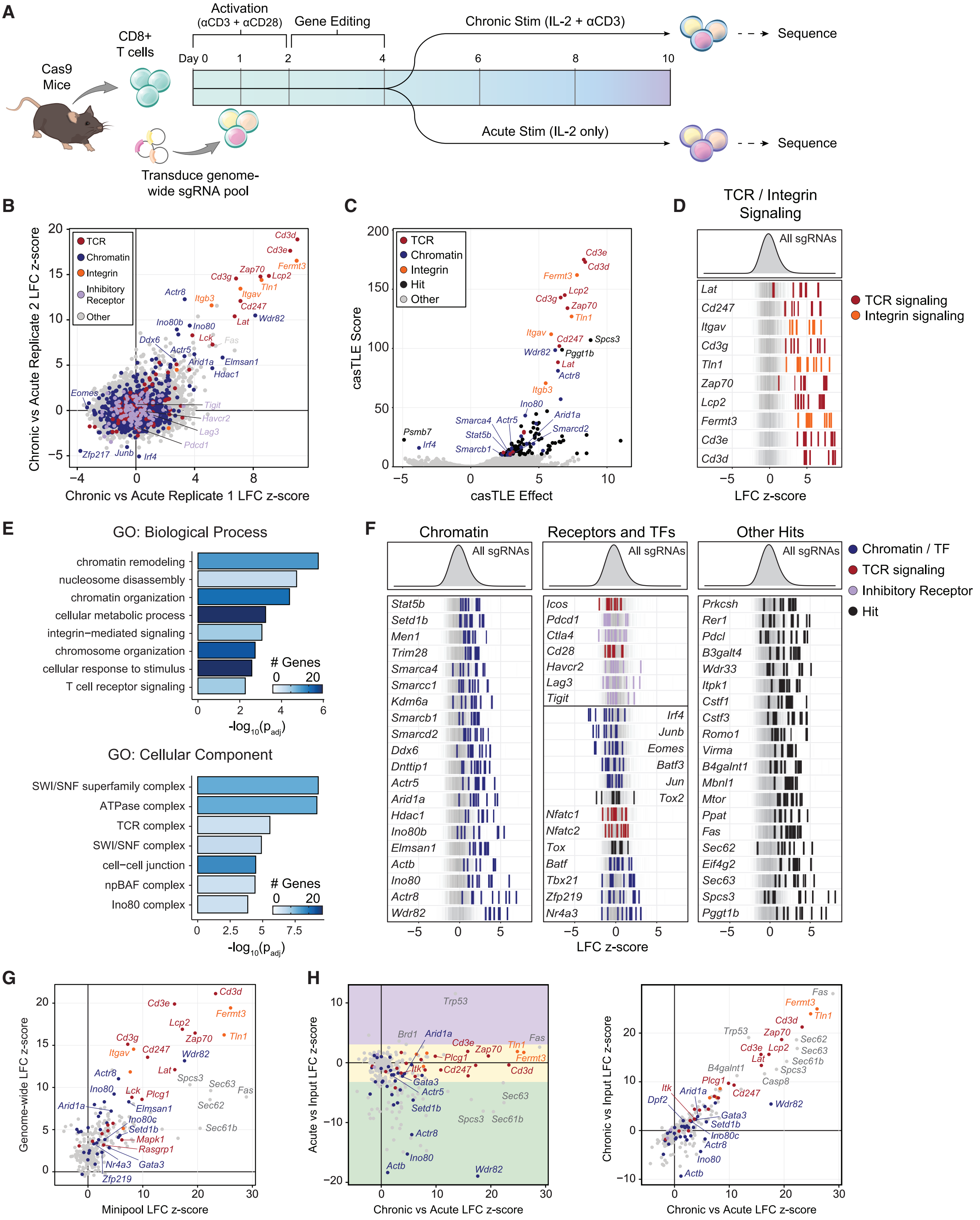

(legend on next page)

Please cite this article in press as: Belk et al., Genome-wide CRISPR screens of T cell exhaustion identify chromatin remodeling factors that limit T cell persistence, Cancer Cell (2022), https://doi.org/10.1016/j.ccell.2022.06.001

motifs, were highly accessible *in vitro* at day 10. Moreover, we observed the progressive loss of accessibility at naive and progenitor exhaustion-associated Lef1 and Tcf7 motifs, early increased accessibility of nuclear factor κB (NF-κB) and Nfat motifs, and later increased accessibility of AP-1 and Nr4a motifs, mirroring the progression of TF activity observed in T cell exhaustion *in vivo* (Figure 1G) (Lynn et al., 2019; Miller et al., 2019; Beltra et al., 2020; Daniel et al., 2021). In summary, these results demonstrate that the *in vitro* T cell exhaustion assay displayed hallmark functional and genomic features of *in vivo* T cell exhaustion.

Genome-wide CRISPR screens identify genetic regulators of T cell exhaustion

We next adapted the *in vitro* exhaustion assay to be compatible with CRISPR screening (Figure 2A). We isolated CD8$^+$ T cells from Rosa26-Cas9 knockin mice, transduced the cells with a genome-wide retroviral sgRNA library containing 90,230 sgRNAs, split the cells into acute (interleukin-2 [IL-2] only) and chronic (anti-CD3 and IL-2) stimulation conditions on day 4, and sequenced both pools on day 10 (Figure 2A) (Platt et al., 2014; Henriksson et al., 2019). We introduced a 48-h delay after activation to allow time for efficient gene editing and puromycin selection of transduced cells and validated that this modified protocol caused similar defects in cytokine production after restimulation (Figures S2A and S2B). We performed replicate screens and confirmed a low multiplicity of infection (MOI), upregulation of inhibitory receptors on day 10 of the chronic culture, and high coverage of the sgRNA library in each condition (Figures S2C–S2F; Table S1). Positive controls for the screen are components of the TCR signaling pathway, since depletion of these factors impairs antigen-driven (or anti-CD3-driven) signaling. Accordingly, we first analyzed the enrichments of the CD3 receptor subunits (*Cd3e*, *Cd3d*, *Cd3g*, *Cd247*; Figure S2G, red) and observed a robust enrichment of guides targeting these genes in both replicates. Merging the replicates yielded an overall *Z* score and ranking for each gene (Figures 2B and 2C; Table S1) (Flynn et al., 2021). We validated this analysis approach by comparing screen hits obtained from two additional CRISPR sgRNA enrichment analytical methods and two normalization strategies (Figures S3A–S3E; Table S2; STAR Methods) (Li et al., 2014; Morgens et al., 2016; Gilbert et al., 2014).

In addition to *Cd3e*, *Cd3d*, and *Cd3g*, top enriched genes in the screen included other known components of the TCR signaling pathway, such as *Zap70*, *Lcp2*, *Lat*, and *Lck*, as well as cell adhesion and integrin-related genes *Fermt3*, *Tln1*, *Itgav*, and *Itgb3* (Figures 2B–2D). Gene Ontology (GO) term analysis of the top 100 positive regulators of exhaustion confirmed that the "TCR signaling pathway" term was highly enriched (p_{adj} = 5.44×10^{-3}; Figure 2E). Surprisingly, in addition to TCR-related GO terms, the other top terms were related to epigenetics, including "chromatin remodeling" (p_{adj} = 1.74×10^{-6}) and "nucleosome disassembly" (p_{adj} = 1.90×10^{-5}; Figure 2E). Indeed, analysis of additional highly enriched genes identified a number of chromatin-related factors, including *Arid1a*, *Smarcc1*, *Smarcd2*, *Ino80*, *Actr8*, and *Actr5* (Figure 2F, left). Of note, the co-stimulatory and inhibitory receptors *Icos*, *Pdcd1*, *Ctla4*, *Cd28*, *Havcr2*, *Lag3*, and *Tigit* were not significantly enriched by the screen (Figure 2F, center). Among TFs, *Irf4*, *Junb*, *Eomes*, and *Batf3* were depleted, while *Tbx21* and *Nr4a3* were modestly enriched, supporting previous demonstrations of their roles in exhaustion (Figure 2F, center) (Ataide et al., 2020; Chen et al., 2019; Paley et al., 2012; Seo et al., 2021). In contrast, *Tox* and *Tox2*, which are critical for the development of exhaustion, were not hits, supporting previous studies demonstrating that deletion of these factors may not improve T cell persistence *in vivo* (Figure 2F, center) (Alfei et al., 2019; Khan et al., 2019; Scott et al., 2019). Similarly, *Jun* and *Batf* were not hits, suggesting that while overexpression of these factors improves T cell persistence, deletion has no significant effect (Lynn et al., 2019; Seo et al., 2021).

We next used Cytoscape to visualize the protein-protein interaction network of top enriched and depleted genes (Figure S4A) (Shannon et al., 2003). This analysis confirmed the highly interconnected and enriched network of factors that directly associate with the TCR complex and downstream signaling components, as well as several other protein complexes and functional categories. These included the INO80 complex (hits included *Ino80*, *Ino80b*, *Ino80c*, *Actr5*, and *Actr8*) and the BRG1/BRM-associated factors (BAF) complex (hits included *Arid1a*, *Smarcb1*, *Smarcd2*, *Smarca4*, and *Smarcc1*)—both ATP-dependent chromatin remodeling complexes that are essential in many aspects of development (Figure S4A; Hargreaves and Crabtree, 2011). Finally, analysis of single-cell RNA-seq (scRNA-seq) data from chronic viral infection showed that nearly all (98/100) top-ranked hits were expressed in exhausted T cells *in vivo* (Figures S4B–S4D) (Raju et al., 2021). In summary, the *in vitro* genome-wide CRISPR-Cas9 exhaustion

Figure 2. Genome-wide functional interrogation of T cell exhaustion

(A) Diagram of genome-wide T cell exhaustion screen.

(B) Correlation of replicate screens (n = 2) with selected functional categories of genes colored as indicated. Gene sets were based on GO terms and were supplemented with manual annotations.

(C) casTLE volcano plot of the chronic versus acute stimulation screen comparison, with top hits labeled.

(D) Individual sgRNA *Z* scores for top hits in "integrin signaling" or "TCR signaling" functional categories.

(E) GO term analysis of the top 100 positive hits.

(F) Individual sgRNA *Z* scores for genes in different functional categories: chromatin (left), selected receptors and transcription factors (center), or other (right). In (D) and (F), n = 10 sgRNA-replicates per gene are shown. A total of 1,000 randomly selected guides are shown in the background of each row in gray, for visual reference.

(G) Correlation of acute versus chronic *Z* scores in the mini-pool versus the genome-wide screen.

(H) Correlation of the mini-pool chronic versus acute *Z* scores against acute versus input (left) or chronic versus input (right).

Genes in (G) and (H) are colored by functional category: TCR signaling (red), integrin signaling (orange), chromatin (blue), or other (gray). Colored boxes in (H, left) denote enhanced (purple), similar (yellow), or reduced (green) expansion after acute stimulation.

See also Figures S2–S5 and Tables S1, S2, and S3.

Please cite this article in press as: Belk et al., Genome-wide CRISPR screens of T cell exhaustion identify chromatin remodeling factors that limit T cell persistence, Cancer Cell (2022), https://doi.org/10.1016/j.ccell.2022.06.001

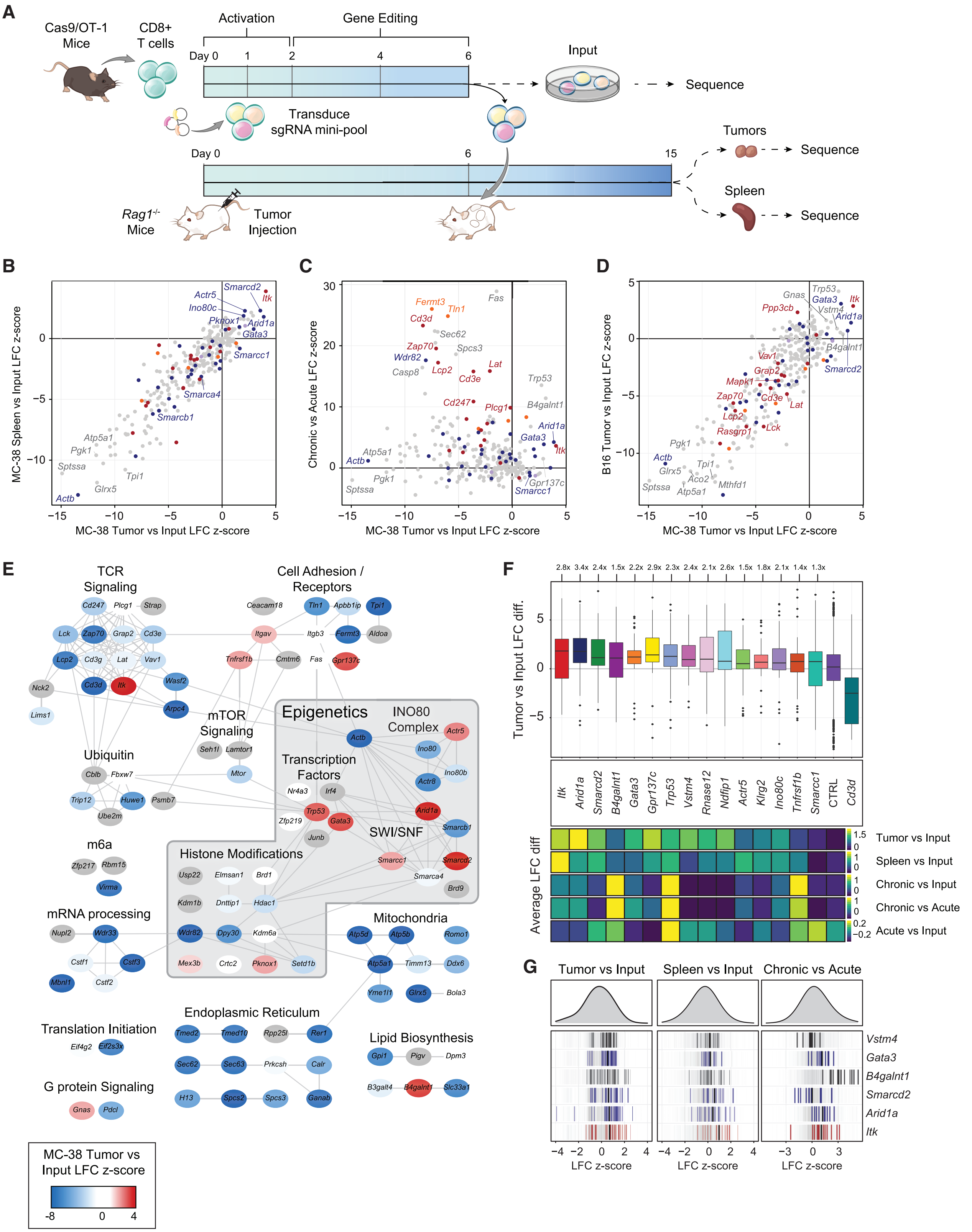

Figure 3. Targeted *in vivo* screening identifies subunits of the INO80 and BAF complexes that limit T cell persistence

(A) Diagram of *in vivo* pooled CRISPR screening.

(B) Correlation of tumor log fold change (LFC) *Z* scores to spleen LFC *Z* scores, colored by functional category.

(legend continued on next page)

Please cite this article in press as: Belk et al., Genome-wide CRISPR screens of T cell exhaustion identify chromatin remodeling factors that limit T cell persistence, Cancer Cell (2022), https://doi.org/10.1016/j.ccell.2022.06.001

screen provides a comprehensive catalog of genetic factors that govern the process of chronic antigen-induced T cell exhaustion and identifies chromatin remodeling factors as potential targets for improving T cell persistence.

Chromatin remodeling factors limit T cell persistence *in vitro* and *in vivo*

To further characterize the top 300 ranked genome-wide screen hits, we created a custom sgRNA mini-pool (Table S2). We repeated the *in vitro* stimulation screen and collected acute and chronic samples, as well as input samples on day 4 (Figure S5A; Table S3). We observed high concordance between biological replicates and therefore merged the replicates (Figures S5B–S5E; Table S3). We considered the chronic versus acute enrichments, which served as validation of the original genome-wide screen. Of the 88 genes in the pool that were statistically significant positive hits in the genome-wide screen, 52 (59.1%) were validated in the mini-pool (FDR <0.05; Figures 2G and S5C). Next, we compared the chronic versus acute gene enrichments to acute versus input or chronic versus input enrichments, which measured the fitness advantage or disadvantage of each gene knockdown relative to the initial pool (Figures 2H and S5E). Most genes displayed either similar (233/300; 77.7%) or reduced (64/300; 21.3%) enrichments in acute stimulation compared to input, enabling the identification of sgRNAs that specifically improve T cell persistence in the presence of chronic antigen, rather than T cell proliferation in general, and that maintain proliferative capacity after acute stimulation (similar: $-3.5 \leq z \leq 3.5$, reduced: $z < -3.5$, improved: $z > 3.5$; Figures 2H, left, and S5E).

To characterize the *in vivo* function of the top hits, we next screened the sgRNA mini-pool in two murine tumor models. On day 0, we bilaterally injected MC-38 colon adenocarcinoma or B16 melanoma tumors that ectopically expressed ovalbumin into Rag1$^{-/-}$ mice and isolated CD8$^+$ T cells from Cas9/OT-1 mice. On day 1, we transduced the T cells with the custom sgRNA mini-pool (Figure 3A). We transplanted 1×10^6 T cells per mouse 6 days after tumor inoculation, harvested the tumors and spleens of mice on day 15, sorted T cells from each organ, and sequenced the bulk sgRNA content in these cells (Figure S6A; Table S3). We computed sgRNA enrichments as described above and merged the results from all of the mice to create an aggregate tumor LFC Z score and spleen LFC Z score for each gene in each tumor model, relative to the control distribution (Figures 3B–3E; Table S3).

Cells containing TCR complex/signaling sgRNAs should have an impaired ability to recognize antigen and thus, in contrast to the *in vitro* screen, were depleted *in vivo*, except for *Itk* (Figure S6B). However, a select group of *in vitro* hits were highly enriched in tumors and spleens in both tumor models, including *Arid1a*, *Itk*, *Smarcd2*, *B4galnt1*, *Gata3*, *Gpr137c*, *Trp53*, and *Vstm4* (Figures 3B–3D). Visualizing the tumor enrichments of each gene in the context of the Cytoscape network revealed that many of the positive hits *in vivo* were epigenetic factors, including subunits of the INO80 complex (*Ino80c* and *Actr5*) and the BAF complex (*Arid1a*, *Smarcd2*, and *Smarcc1*; Figure 3E). The top-ranked gene knockdowns improved T cell accumulation in tumors by up to 3.4-fold. For comparison, T cells lacking *Cd3d* were depleted 6.7-fold and T cells lacking *Cd3e* were depleted 3.3-fold, demonstrating that targeting the top hits substantially improved T cell persistence in tumors (Figures 3F and S6C). These results validate the genome-wide screen, identify perturbations that improve T cell persistence only in the setting of chronic antigen stimulation, rather than improving general T cell fitness, and nominate the BAF and INO80 complexes for further investigation (Figures 3F, 3G, and S6C).

Tuning cBAF activity enhances T cell persistence and improves tumor control

We next validated the persistence advantage of *Arid1a*-sgRNA cells (the top epigenetic hit in the screen). We used a cell competition assay in which cells were transduced with either a single-targeting control (CTRL1) sgRNA or an *Arid1a*-targeting sgRNA with different fluorescent reporters (STAR Methods), mixed, and then put into the *in vitro* chronic stimulation assay (Figure 4A) or the *in vivo* MC-38 tumor model (Figure 4B). The activity of both *Arid1a*-targeting sgRNAs was confirmed at the DNA and protein levels (Figures S6D–S6F). *In vitro* and *in vivo*, *Arid1a*-sgRNA cells demonstrated significantly enhanced persistence, compared to control cells, confirming the results of the pooled screens (Figures 4A and 4B). Moreover, *Arid1a*-sgRNA cells exhibited lower surface protein expression of PD-1 and TIM3 after chronic stimulation *in vitro* (Figure 4A). Finally, we evaluated whether the observed enhanced persistence of *Arid1a*-sgRNA cells resulted in improved antitumor responses *in vivo*. We inoculated Rag1$^{-/-}$ mice with MC-38 tumors as previously described, and on day 6, transplanted 5×10^5 Cas9/OT-1 CD8$^+$ T cells transduced with either CTRL1 retrovirus or *Arid1a*-sgRNA retrovirus and monitored tumor growth (Figure 4C). By day 15, the transfer of *Arid1a*-sgRNA cells significantly improved tumor clearance, compared to the transfer of control cells (*Arid1a*-sgRNA versus CTRL1 tumor size, day 15: $p = 5 \times 10^{-8}$; Welch two-sample t test). Importantly, survival of mice receiving *Arid1a*-sgRNA T cells was significantly extended, compared to mice receiving CTRL1 T cells (median survival = 12 days [no transplant], 15 days [CTRL1], 25 days [*Arid1a*-sgRNA]; *Arid1a*-sgRNA versus CTRL1: $p = 1.20 \times 10^{-8}$; Figure 4D).

(C) Correlation of *in vivo* Z scores and *in vitro* Z scores for genes in the CRISPR mini-pool.
(D) Correlation of *in vivo* MC-38 and B16 tumor Z scores for genes in the CRISPR mini-pool.
(B–D) Results shown are merged from 3 mice per tumor model (n = 6 tumors, n = 3 spleens).
(E) Cytoscape protein-protein interaction network colored by Z scores in MC-38 tumors.
(F) Top: Boxplot of MC-38 tumor versus input LFC for each sgRNA targeting the indicated gene, with the mean control LFC subtracted. Bottom: Heatmaps showing the sgRNA average of the indicated *in vivo* or *in vitro* screen for the same hits. Boxplots show 25th, 50th (median), and 75th percentiles, with outliers shown as dots. Each dot represents 1 sgRNA replicate, n = 36 per target gene.
(G) Individual sgRNA replicate Z scores for 6 top hits showing the MC-38 tumor versus input comparison (left, n = 36), MC-38 spleen versus input (center, n = 18), and *in vitro* chronic versus acute (right, n = 12).
See also Figure S6 and Tables S2 and S3.

Please cite this article in press as: Belk et al., Genome-wide CRISPR screens of T cell exhaustion identify chromatin remodeling factors that limit T cell persistence, Cancer Cell (2022), https://doi.org/10.1016/j.ccell.2022.06.001

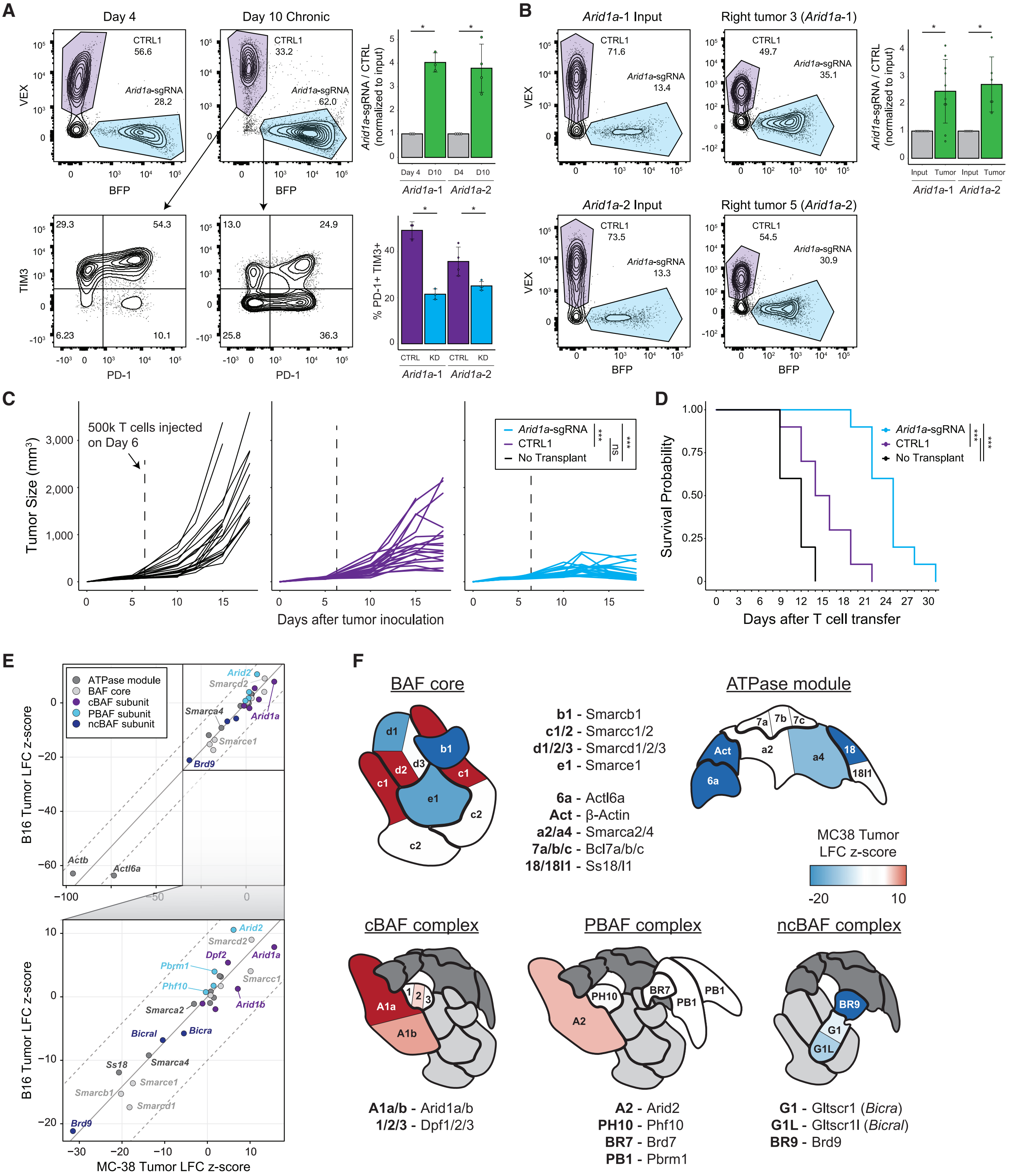

Figure 4. SWI/SNF mini-pool CRISPR screens and functional studies demonstrate that tuning cBAF activity can enhance antitumor immunity

(A) *In vitro* competition assay of *Arid1a*-sgRNA versus CTRL1 T cells. Left: Cells were mixed on day 4 at the indicated ratios and passaged in the chronic stimulation assay for 6 days. On day 10, proliferation relative to CTRL1 T cells and surface phenotype was assessed by flow cytometry, n = 3 or 4 as indicated.

(B) *In vivo* competition assay of *Arid1a*-sgRNA versus CTRL1 T cells. Cells were mixed on day 6 (input) and then transplanted into tumor-bearing mice. On day 15, relative proliferation in the tumor was assessed by flow cytometry, n = 6 or 10, as indicated.

(A and B) Error bars denote means ± SDs and significance was assessed by Welch 2-sample t test.

(C) Tumor sizes for each cohort. Statistical significance was assessed at day 15 by Wilcoxon rank-sum exact test, n = 20 tumors per group.

(legend continued on next page)

Please cite this article in press as: Belk et al., Genome-wide CRISPR screens of T cell exhaustion identify chromatin remodeling factors that limit T cell persistence, Cancer Cell (2022), https://doi.org/10.1016/j.ccell.2022.06.001

To provide deeper mechanistic insight into the role of BAF complex factors in T cell exhaustion, we performed an additional CRISPR mini-pool screen targeting each of the 29 SWI/SNF complex subunit genes in the B16 and MC-38 tumor models and interpreted these results in the structural context of SWI/SNF complex assembly (Mashtalir et al., 2018) (Table S2). As observed in the prior *in vivo* screen, the three most significant hits were in the cBAF complex (*Arid1a*, *Smarcc1*, and *Smarcd2*) and notably were in positions of the complex that can be substituted by paralogs in other forms of the complex (Figures 4E and 4F; Table S4) (Mashtalir et al., 2018). In contrast, perturbation of the irreplaceable subunits of the BAF core (e.g., *Smarce1*, *Smarcb1*) or ATPase module components was deleterious and led to the depletion of these sgRNAs. Therefore, we propose a model in which tuning (reducing) the presence of cBAF on chromatin is beneficial for T cell persistence. This concept is supported by prior mechanistic studies demonstrating that *ARID1A*-deficient tumors exhibit reduced (but not ablated) levels of cBAF complex on chromatin, which results in the decreased access of key transcription factors (including AP-1 factors) (Mathur et al., 2017; Xu et al., 2020). In addition to cBAF, we also observed positive enrichments of sgRNAs targeting the PBAF complex member *Arid2* and strong depletion of sgRNAs targeting the ncBAF complex members *Bicral*, *Bicra*, *and Brd9* (Figures 4E and 4F; Table S4). In summary, these results demonstrate that perturbation of cBAF complex subunit genes can improve T cell persistence and antitumor immunity *in vivo*.

Perturbation of *ARID1A* improves T cell persistence in primary human T cells

We asked whether perturbation of cBAF subunits could also improve the persistence of primary human T cells in an *in vitro* chronic stimulation assay (Figure 5A). We introduced CRISPR-Cas9 sgRNA ribonucleoproteins (RNPs) targeting *ARID1A* (two independent sgRNAs) or a control RNP into primary human T cells. We split the cells into acute and chronic cultures, and the chronic condition was stimulated for 6 days with anti-CD3-coated plates. In acutely stimulated cultures, we observed no difference between the genotypes for proliferation or viability. However, in chronically stimulated cultures, *ARID1A*-sgRNA cells proliferated significantly more and maintained higher viability than CTRL T cells (*ARID1A*-sgRNA versus CTRL1 cells: mean increase of 5.25-fold expansion, $p = 0.013$; Figure 5A).

We next validated the persistence advantage of *ARID1A*-sgRNA T cells *in vivo*. We designed a CRISPR mini-pool for *in vivo* human T cell experiments, which encompassed 48 sgRNAs targeting 20 genes and included 8 negative control guides (Table S5). We included sgRNAs targeting *ARID1A*, as well as the inhibitory receptors *PDCD1*, *LAG3*, and *HAVCR2*, and other top-ranked genes from our prior screens, such as *TMEM222*, *CBLB*, *TCEB2*, and *SOCS1* (Shifrut et al., 2018). We performed the screen in the A375 human melanoma xenograft model, which expresses the NY-ESO-1 antigen. We introduced the cognate 1G4 TCR into primary human T cells on day 1 along with the sgRNAs and transplanted T cells into NOD-SCID-IL2Rγ-null (NSG) tumor-bearing mice on day 14 (Figure 5B). Seven days later, we sorted T cells from the tumors and spleens, sequenced the sgRNAs present in each organ, and compared their abundance to input samples before transplant. As expected, we did not observe enrichments in control sgRNAs or sgRNAs targeting inhibitory receptors but we did observe the depletion of sgRNAs targeting *CD3D* (Figures 5C and 5D). In contrast, sgRNAs targeting *ARID1A* were significantly enriched in tumors compared to input samples in both donors, demonstrating that the function of cBAF in limiting T cell persistence is conserved in human T cells (*ARID1A*-sgRNA versus CTRL LFC: $p = 0.0010$ by Wilcoxon test; Figures 5C and 5D).

In vivo Perturb-seq reveals distinct transcriptional effects of chromatin remodeling complexes in TILs

To understand the molecular mechanisms driving improved T cell function in hits identified by the CRISPR screens, we performed Perturb-seq, which simultaneously captures CRISPR sgRNAs and the transcriptome in single cells (Adamson et al., 2016; Dixit et al., 2016; Replogle et al., 2020). We designed a third custom sgRNA pool (micro-pool) targeting the INO80 and BAF complexes. For SWI/SNF genes, we targeted *Arid1a*, *Smarcc1*, and *Smarcd2* (top hits identified *in vitro* and *in vivo)*, as well as *Arid2* and *Arid1b*, which were enriched in the SWI/SNF-specific mini-pool screen. From the INO80 complex, we selected *Actr5* and *Ino80c*, which were enriched in both the *in vitro* and *in vivo* screens. Finally, we included positive controls *Pdcd1* and *Gata3*, as well as 12 single targeting negative controls for a total of 48 sgRNAs targeting 9 genes (Table S2). We performed a similar *in vivo* T cell protocol as described above for the larger CRISPR screen, including collecting an input sample to evaluate the persistence phenotype of each sgRNA. Nine days after T cell transplantation, we harvested tumors, isolated TILs, and used direct-capture Perturb-seq to simultaneously readout sgRNA identity and scRNA-seq profile (Figures 6A, S7A, and S7B) (Replogle et al., 2020).

After quality control filtering, we obtained high-quality scRNA-seq profiles from 70,646 cells and identified 6 clusters (Figure 6B). We determined a high-confidence sgRNA identity for 52,607 cells (74.4%; Figure 6C; STAR Methods). Cell-type clusters expressed varied levels of inhibitory receptors, effector cytokines, and key transcription factors, indicating that they represented a mix of exhausted and effector T cells (Figures 6D, S7C, and S7D). Cluster 1 expressed high levels of *Klf2* and *S1pr1* (T effector memory [T_{EM}]); cluster 2 expressed high levels of IFN-stimulated genes (ISGs) such as *Mx1* (T_{ISG}); cluster 3 expressed high levels of *Tnfrsf9* (encoding 41BB) and *Cd160* (T-41BB); cluster 4 expressed high levels of progenitor exhaustion genes, including *Pdcd1*, *Tcf7*,

---

(D) Survival curves of tumor-bearing mice in each treatment group. Statistical significance was assessed by log-rank test, n = 10 mice per group.

(E) Correlation of SWI/SNF CRISPR mini-pool tumor enrichments in MC-38 versus B16 tumor models. Results shown are merged from 4 mice for MC-38 (n = 8 tumors, n = 4 spleens) or 2 mice for B16 tumors (n = 4 tumors, n = 2 spleens).

(F) Illustrations of the 3 BAF complexes colored by *Z* score from SWI/SNF CRISPR mini-pool experiments in MC-38 tumors. BAF complex illustrations adapted from Mashtalir et al. (2018). *$p < 0.05$, ***$p < 0.001$.

See also Figure S6 and Table S4.

Please cite this article in press as: Belk et al., Genome-wide CRISPR screens of T cell exhaustion identify chromatin remodeling factors that limit T cell persistence, Cancer Cell (2022), https://doi.org/10.1016/j.ccell.2022.06.001

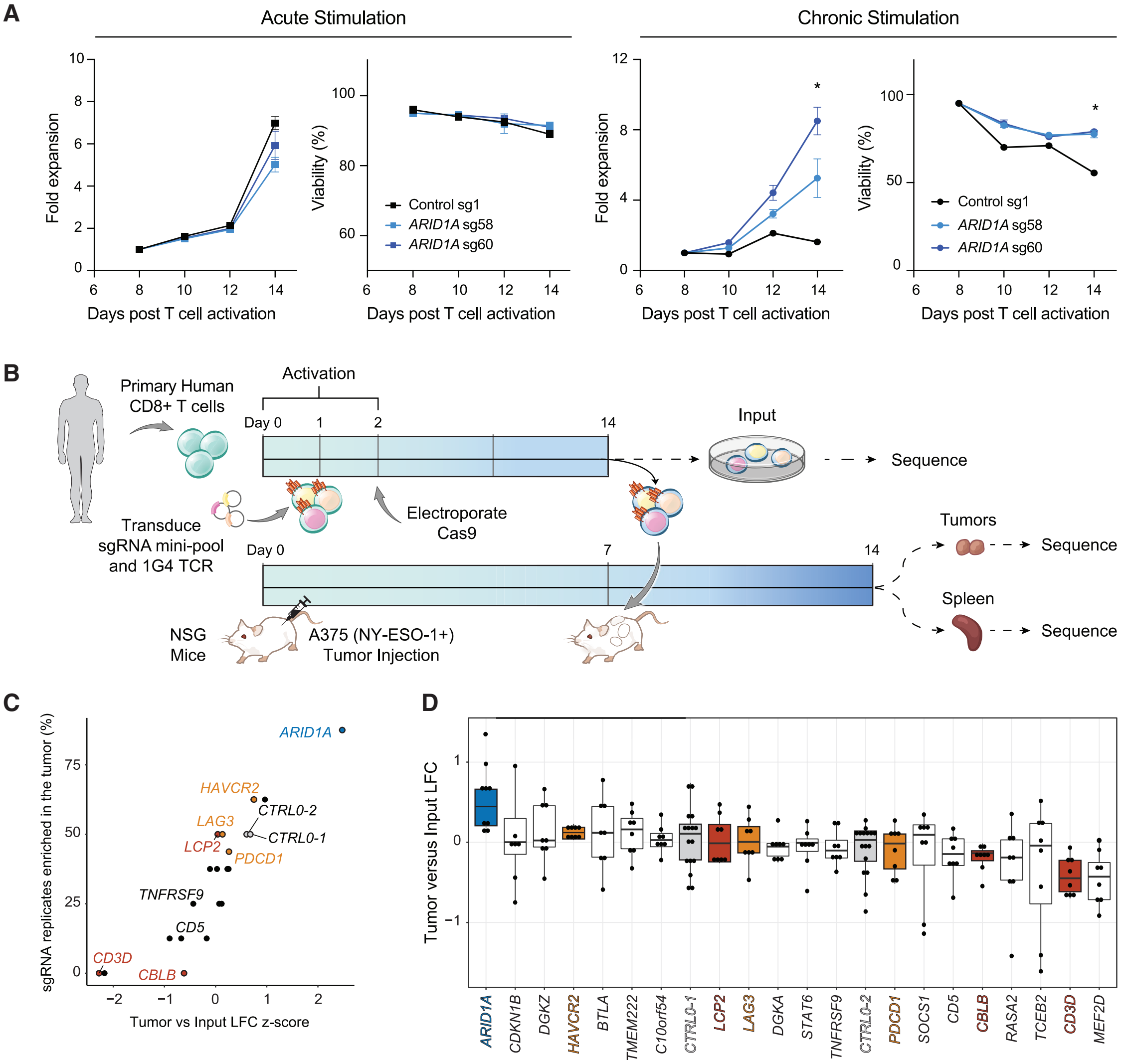

Figure 5. Conserved function of *ARID1A* in human T cells *in vitro* and *in vivo*

(A) Proliferation and viability of primary human T cells after electroporation of the indicated RNP. Left: Acutely stimulated T cells. Right: Chronically stimulated T cells using anti-CD3-coated plates. Data shown are representative of 3 independent experiments and 3 donors. Error bars denote means ± SDs and significance was assessed by Student's t test, n = 2 replicates per sgRNA.

(B) Schematic of CRISPR mini-pool screen in primary human CD8$^+$ T cells transduced with the NY-ESO-1-specific TCR, 1G4.

(C) Results of the human CRISPR mini-pool screen aggregated by gene.

(D) Results of the human CRISPR mini-pool screen with individual sgRNA replicates shown as dots. Genes are ordered from highest to lowest average LFC. Boxplots show 25th, 50th (median), and 75th percentiles.

Results shown in (C) and (D) are combined from 2 independent donors, 2 mice per donor, and 2 sgRNAs per target gene (n = 8 sgRNA replicates per target). In (C) and (D), orange indicates inhibitory receptors, red indicates TCR signaling pathway genes, blue indicates chromatin remodelers, and gray indicates negative controls.

See also Table S5.

and *Slamf6* (T_{EX}Prog); cluster 5 expressed the highest levels of inhibitory receptors *Pdcd1*, *Lag3*, and *Havcr2* (T_{EX}Term); and cluster 6 consisted primary of cycling cells, marked by *Mki67* and confirmed by cell-cycle analysis (T-cycling; Figures S7C and S7D). To confirm cluster identities, we generated gene signatures from previously published CD8$^+$ T cell types present in acute or chronic LCMV infection *in vivo* (Figures S7E and S7F; STAR Methods) (Daniel et al., 2021). We used the top 100 marker genes for each LCMV T cell cluster to score each single cell in our Perturb-seq dataset according to the average expression of these signature gene sets. Visualizing the enrichment of these LCMV signatures in each cluster demonstrated transcriptional similarity of several clusters to cell types in the reference dataset (Figure 6E). For example, cluster 1 was enriched for the effector memory-related genes (T_{EM} signature), cluster 2 was similar to the T_{EX}ISG signature, and the progenitor and terminally exhausted clusters (clusters 4 and 5) enriched the corresponding LCMV signatures (Figure 6E).

We performed sgRNA-level quality controls to assess the reproducibility of effects of independent sgRNAs (Figures 6F

Please cite this article in press as: Belk et al., Genome-wide CRISPR screens of T cell exhaustion identify chromatin remodeling factors that limit T cell persistence, Cancer Cell (2022), https://doi.org/10.1016/j.ccell.2022.06.001

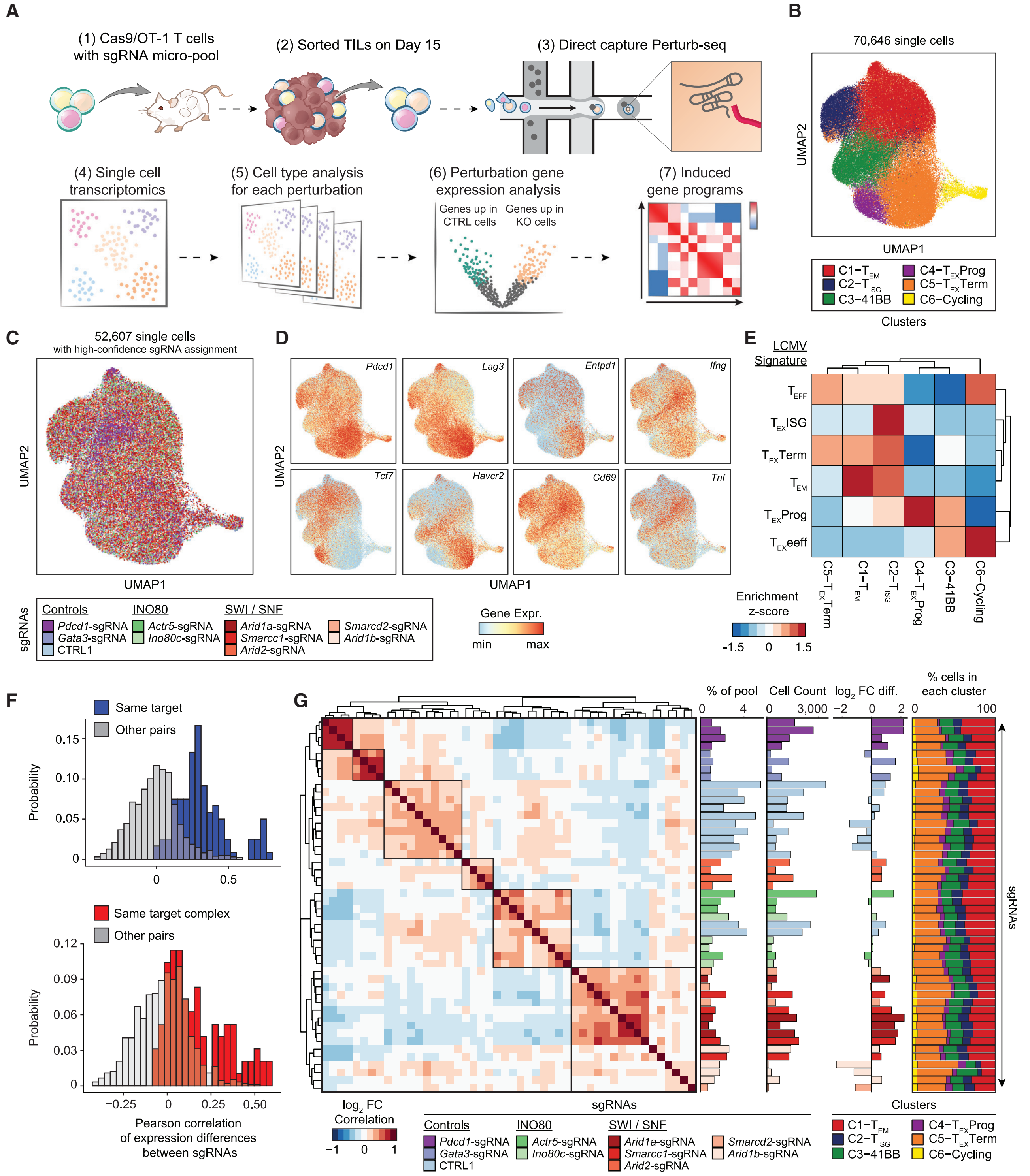

Figure 6. *In vivo* Perturb-seq reveals distinct transcriptional roles of the cBAF and INO80 complexes in TILs
(A) Diagram of direct-capture Perturb-seq of sorted TILs.
(B) scRNA-seq profiles of TILs colored by cluster assignment.
(C) scRNA-seq profiles of cells colored by the perturbation detected in each cell. Cells where no guide, or multiple guides, were detected are shown in gray.
(D) Expression of selected marker genes in each single cell.
(E) Analysis of LCMV signature gene sets for each cluster. Gene set enrichment scores were calculated for each single cell; cell values were averaged by cluster and *Z* scored.

(legend continued on next page)

Please cite this article in press as: Belk et al., Genome-wide CRISPR screens of T cell exhaustion identify chromatin remodeling factors that limit T cell persistence, Cancer Cell (2022), https://doi.org/10.1016/j.ccell.2022.06.001

and 6G). We first computed gene expression differences between each sgRNA and all other cells in the dataset. Independent sgRNAs targeting the same gene had highly correlated gene expression changes, relative to pairs of sgRNAs targeting different genes (Figures 6F and 6G). Interestingly, pairs of sgRNAs targeting the same complex (grouping together sgRNAs targeting cBAF genes or sgRNAs targeting INO80 genes) also induced highly correlated changes, indicating common transcriptional effects of targeting distinct subunits within the same complex (Figures 6F and 6G). *Arid2* clustered separately from the rest of the BAF-targeted sgRNAs, suggesting distinct roles for the cBAF and PBAF complexes (Figure 6G). We next used the input representation of each sgRNA to estimate the T cell accumulation advantage of each sgRNA relative to controls, which demonstrated that the majority of sgRNAs enhanced T cell accumulation in the tumor, relative to control sgRNAs, in line with the *in vivo* screen results (Figure 6G). In particular, *Arid1a*-sgRNA cells were enriched 2.74-fold on average relative to CTRL1 cells (Figure 6G). Finally, we examined the cell-type cluster composition of cells containing each sgRNA (Figure 6G, far right). All of the perturbations contained cells from each cluster with similar proportions, suggesting that depletion of each target gene may not affect wholescale changes in cell-type composition, but rather modulates gene expression in one or more clusters.

To further investigate this possibility, we aggregated cells that contained sgRNAs targeting the same gene and computed differential gene expression for each perturbation, compared to CTRL1 cells (Figures 7A–7F; Table S6). Targeting cBAF subunits *Arid1a*, *Smarcd2*, or *Smarcc1* induced shared global changes in the transcriptional program of T cells, including the upregulation of effector molecules *Gzmb* and *Ifng*, cell surface receptors *Cxcr6* and *Il7r*, and TFs *Irf4* and *Batf*. Meanwhile, *Pdcd1*, *Lag3*, and *Ccl5* were consistently downregulated by cBAF perturbation (Figures 7A–7F). In contrast, *Arid2* perturbation induced a distinct gene expression program, albeit with some similarities, including the downregulation of *Pdcd1* and *Lag3*. Perturbation of *Gata3* and *Pdcd1* induced distinct gene expression changes from either cBAF or *Arid2* perturbation; for example, the most upregulated gene after *Pdcd1* depletion was *Tox*, perhaps consistent with the proposed impact of PD-1 deletion on accelerating differentiation to terminal exhaustion (Figures 7A–7F) (Odorizzi et al., 2015). Finally, when gene expression changes were analyzed within each cluster, we found that each perturbation induced highly concordant changes in gene expression regardless of the T cell subtype (Figure S7G). GO term analysis of the cBAF upregulated gene set enriched effector terms, including T cell activation, cell adhesion, cytokine production, and T cell proliferation (Figure 7H). In contrast, INO80 perturbation substantially modulated metabolism-related genes (Figures 7E and 7H). The projection of genes upregulated by cBAF depletion onto canonical T cell states identified in chronic LCMV infection showed an enrichment in effector T cell clusters, while the projection of downregulated genes showed an enrichment in terminally exhausted T cell clusters (Figures 7G and S8B). In summary, these data demonstrate that subunits of the cBAF and INO80 chromatin remodeling complexes have distinct roles in T cell exhaustion that are largely conserved within the same complex, with cBAF primarily regulating effector- and exhaustion-related genes and INO80 regulating metabolism. Furthermore, the transcriptional impact of targeting chromatin remodeling factors minimally overlaps with the impact of previously known targets, *Pdcd1* and *Gata3*, suggesting the potential to synergistically target multiple pathways to improve T cell function (Figures 7F and S8A).

Arid1a perturbation limits the acquisition of terminal exhaustion-associated chromatin accessibility

We next asked how perturbation of *Arid1a* affected the epigenetic landscape of T cell exhaustion. We performed a competition assay as described above, wherein CTRL1 and *Arid1a*-sgRNA cells were mixed and subjected to *in vitro* exhaustion. At days 6 and 10, we isolated CTRL1 and *Arid1a*-sgRNA cells from the same culture and performed ATAC-seq on each population. To analyze these results in the context of our initial assay characterization (Figure 1), we included the profiles of naive (day 0) and activated (day 2) wild-type (WT) T cells (Figure 8A). The chromatin state progression in CTRL1 cells proceeded similarly to that observed previously in unperturbed cells; however, *Arid1a*-sgRNA cells proceeded down a distinct trajectory, remaining closer to naive and activated samples than the CTRL1 cells at both time points (Figure 8A).

We defined regulatory elements as "opened" peaks if we observed increased accessibility at day 10, compared to day 6, and as "closed" peaks if we observed decreased accessibility at day 10, compared to Day d ($p_{adj} < 0.05$, LFC > 1). Analysis of these peak sets demonstrated substantially different chromatin remodeling changes in *Arid1a*-sgRNA T cells, compared to CTRL1 T cells (Figures 8B and 8C). First, *Arid1a*-sgRNA cells exhibited a marked global decrease in the number of opened peaks, likely representing a relative inability of cBAF-depleted cells to establish accessible chromatin (Figure 8B). Second, while *Arid1a*-sgRNA cells and CTRL1 cells closed chromatin to a similar extent, the majority of these regions were non-overlapping (Figure 8B). Analysis of individual exhaustion-associated regulatory elements, including those in *Pdcd1*, *Lag3*, *Entpd1*, and *Ifng* gene loci, revealed a substantial loss of accessibility in *Arid1a*-sgRNA cells, compared to CTRL1 cells (Figure 8D). Analysis of the terminal T_{EX}-specific peak set (defined in Figure 1) showed that these sites were significantly less accessible in *Arid1a*-sgRNA cells than in CTRL1 cells at both time points

---

(F) Histogram of Pearson correlation of gene expression differences of pairs of sgRNAs. Top: Pairs targeting the same gene are shown in blue (n = 120); other pairs are shown in gray (n = 1,008). Bottom: Pairs targeting the same protein complex are shown in red (n = 96); other pairs are shown in gray (n = 912). Complexes considered in the analysis are cBAF (*Arid1a*, *Arid1b*, *Smarcd2*, and *Smarcc1*) and INO80 (*Ino80c* and *Actr5*), and pairs of sgRNAs that target the same gene are excluded.

(G) Left: Heatmap of the correlation of gene expression differences of each pair of sgRNAs. Center (from left to right): Representation of each sgRNA in the pre-transplant sample, cell count of each sgRNA in the Perturb-seq dataset, and estimated FC of each sgRNA relative to controls. Right: Proportion of cells in each cluster for each sgRNA.

See also Figure S7.

Please cite this article in press as: Belk et al., Genome-wide CRISPR screens of T cell exhaustion identify chromatin remodeling factors that limit T cell persistence, Cancer Cell (2022), https://doi.org/10.1016/j.ccell.2022.06.001

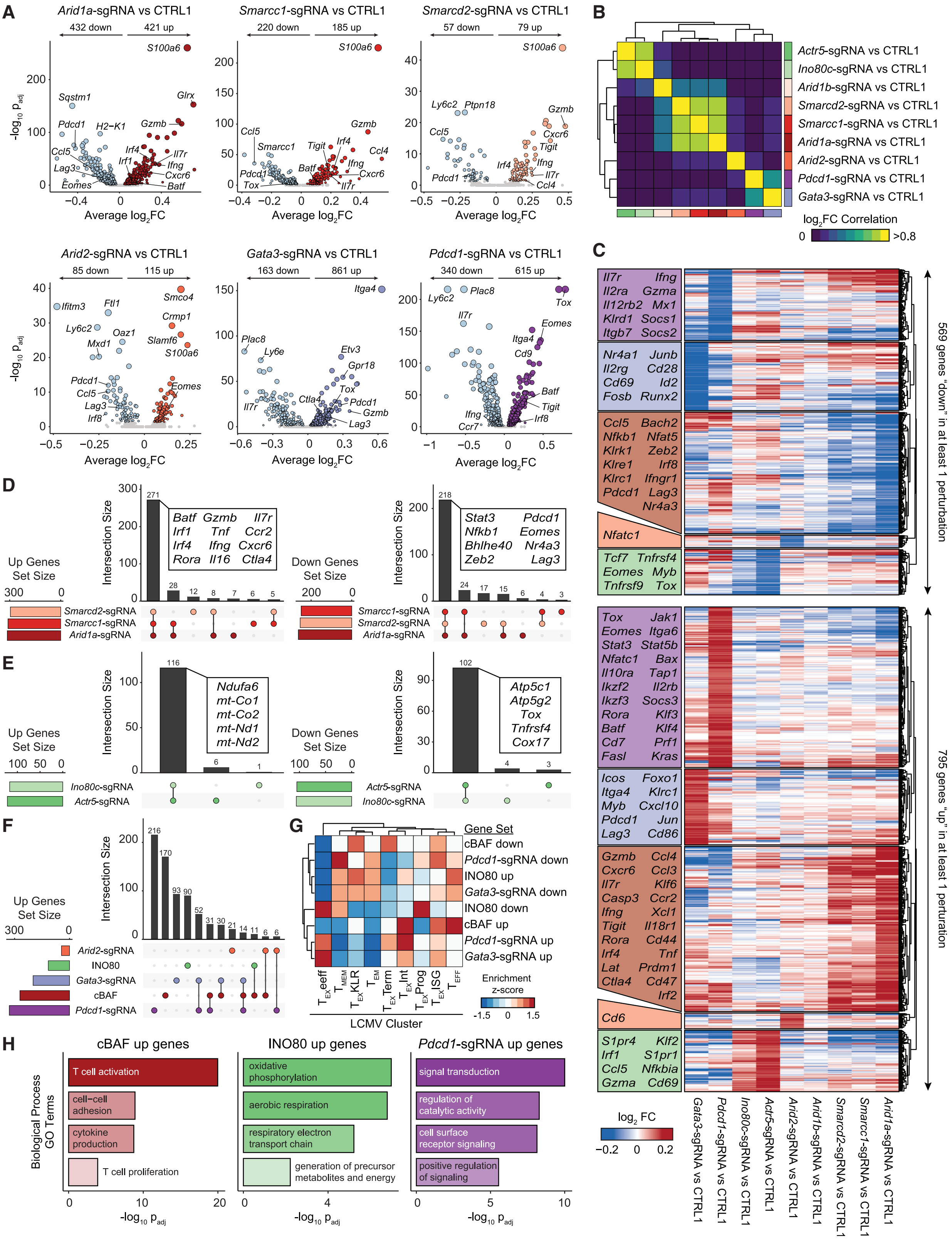

(legend on next page)

Please cite this article in press as: Belk et al., Genome-wide CRISPR screens of T cell exhaustion identify chromatin remodeling factors that limit T cell persistence, Cancer Cell (2022), https://doi.org/10.1016/j.ccell.2022.06.001

(Figures 8E, S8C, and S8D). We next analyzed chromatin accessibility at TF binding sites, which showed that terminal exhaustion-associated TF motifs, including Fos, Jun, and AP-1 motifs were significantly less accessible in *Arid1a*-sgRNA cells, compared to CTRL1 cells (Figure 8F). Conversely, several TF motifs associated with effector T cell function, including Ets, Klf, and Irf motifs, showed increased accessibility in *Arid1a*-sgRNA cells. Finally, ATAC-seq analysis of chronically stimulated *ARID1A*-sgRNA human T cells demonstrated a similar loss of global chromatin accessibility at AP-1 motifs, compared to control T cells, supporting the conserved epigenetic function of *ARID1A* in human T cells (Figures S8E–S8G). In summary, these results suggest that the depletion of cBAF subunits, including *Arid1a*, may improve T cell function by restricting the access of AP-1 TFs to chromatin and thereby preventing the acquisition of the terminal exhaustion-associated chromatin state.

DISCUSSION

In this study, we performed genome-wide CRISPR screens in chronically stimulated T cells, which provide a comprehensive atlas of genes that regulate T cell exhaustion. We used a complementary *in vitro* and *in vivo* screening strategy: (1) the development of an *in vitro* exhaustion assay that is compatible with genome-wide CRISPR screening enabled us to scale the number of cells and sgRNA library coverage compared to prior screens, providing an unbiased discovery tool, and (2) *in vivo* follow-up screens identified perturbations that significantly improved T cell persistence in immunotherapy-relevant tumor models. Importantly, this strategy recovered known regulators of exhaustion, including *Gata3*, which has been demonstrated to limit T cell function in tumor models (Singer et al., 2016). However, these screens also uncovered new genes, with a surprising enrichment of epigenetic factors involved in chromatin and nucleosome remodeling, including the cBAF and INO80 complexes. *In vivo* Perturb-seq experiments revealed that depletion of cBAF and INO80 complex subunits affected distinct gene programs: cBAF perturbation led to the upregulation of an effector program and downregulation of terminal exhaustion genes, while INO80 perturbation primarily affected gene expression related to metabolic function. Finally, depletion of the cBAF complex subunit *Arid1a* improved T cell persistence in *in vitro* and *in vivo* competition assays and improved antitumor immunity after adoptive T cell transfer.

Our strategy was to isolate a key determinant of T cell dysfunction in cancer—chronic stimulation through the TCR—from the multifactorial process involving tumor localization, trafficking, and immunosuppressive effects in the TME. The advantage of this strategy is its specificity; sgRNA abundance is affected by a single selection factor, and therefore, we provide a precise conceptual picture of the molecular drivers of T cell exhaustion. For example, T cell inhibitory receptors such as PD-1 and CTLA-4 were not hits in our screen, supporting the notion that checkpoint blockade does not work by reversing or preventing the process of T cell exhaustion, but rather by recruiting new functional T cell clones to enter the TME (Yost et al., 2019, 2021; Pauken et al., 2016; Spitzer et al., 2017). However, we wish to acknowledge that this strategy does not account for additional dysfunction pathways in T cells that may be mediated by other external stimuli, for example transforming growth factor β (TGF-β)-mediated suppression, or metabolic or nutrient stressors (Mariathasan et al., 2018; DePeaux and Delgoffe, 2021). Similarly, our follow-up *in vivo* screen selected for one functional aspect of exhaustion—T cell persistence in tumors—but did not account for additional aspects, such as cytokine secretion, and thus, additional genes identified in the *in vitro* screen may be uncovered as important regulators of other facets of T cell exhaustion in future studies.

The enrichment of chromatin remodeling factors as hits in both *in vitro* and *in vivo* screens provides a complementary message to previous epigenomic profiling studies in T cell exhaustion (Pauken et al., 2016; Sen et al., 2016; Philip et al., 2017; Scott-Browne et al., 2016). Namely, these prior studies demonstrated that exhaustion is mediated by global chromatin remodeling, which maintains a stable dysfunctional cellular phenotype that is not altered by anti-PD-1 treatment. We now show that targeting nucleosome remodeling complexes may be sufficient to prevent the acquisition of features of this exhaustion-associated chromatin state, and thereby improve T cell persistence and maintenance of an effector-like state. It is possible that deletion of these factors may "dampen" the downstream epigenetic impact of chronic TCR signaling and extend the window in which T cells can engage antigens without accumulating exhaustion-associated epigenetic changes. Recent studies in fibroblasts have demonstrated that AP-1 family TFs may play an essential role in signal-dependent enhancer selection by collaboratively binding to nucleosomal enhancers and recruiting the BAF complex to establish accessible chromatin (Vierbuchen et al., 2017). Indeed, analysis of *Arid1a*-sgRNA T cells revealed a dramatic

Figure 7. cBAF-depleted T cells exhibit enhanced effector gene signatures and reduced terminal exhaustion

(A) Volcano plots comparing aggregated cells with the indicated perturbation versus CTRL1 cells. FDR values were calculated via Wilcoxon rank-sum test, as implemented in Seurat. Sample size: n = 4,668 (*Arid1a*-sgRNA), n = 5,891 (*Smarcc1*-sgRNA), n = 1,448 (*Smarcd2*-sgRNA), n = 3,712 (*Arid2*-sgRNA), n = 2,625 (*Gata3*-sgRNA), n = 6,465 (*Pdcd1*-sgRNA), and n = 18,569 (CTRL1).

(B) Pairwise correlations of gene expression differences induced by each perturbation.

(C) Heatmap of all upregulated (up) or downregulated (down) genes in at least 1 perturbation, grouped by which perturbation has the strongest effect on expression. Selected genes in each block are labeled.

(D) Comparison of upregulated or downregulated gene sets by perturbation of cBAF subunits, *Arid1a*, *Smarcd2*, or *Smarcc1*.

(E) Comparison of gene sets up- or downregulated by perturbation of INO80 subunits *Actr5* or *Ino80c*.

(F) Comparison of gene sets upregulated by perturbation of cBAF subunits, INO80 subunits, or *Pdcd1*, *Gata3*, or *Arid2*.

(G) Enrichments of upregulated and downregulated gene sets in LCMV expression data (Daniel et al., 2021). Module scores of each gene set were computed for each single cell in the LCMV dataset, averaged by cluster, and then *Z* scored to obtain the indicated enrichment *Z* scores.

(H) Selected GO terms of indicated gene sets.

See also Figure S8 and Table S6.

Please cite this article in press as: Belk et al., Genome-wide CRISPR screens of T cell exhaustion identify chromatin remodeling factors that limit T cell persistence, Cancer Cell (2022), https://doi.org/10.1016/j.ccell.2022.06.001

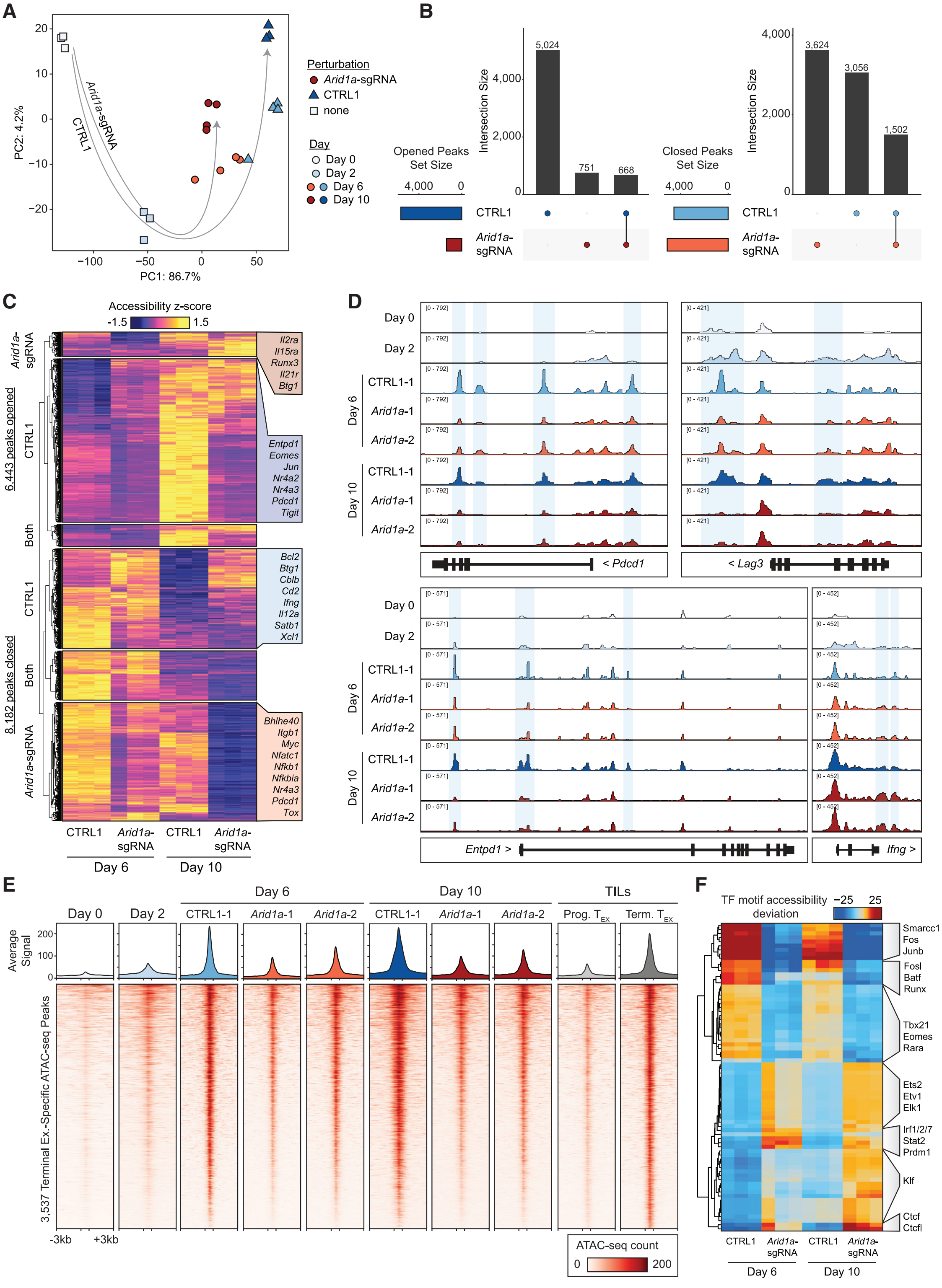

Figure 8. *Arid1a* is required for the acquisition of the exhausted T cell chromatin state

(A) Principal-component analysis of ATAC-seq profiles of *Arid1a*-sgRNA and CTRL1 cells in the *in vitro* exhaustion competition assay (n = 3 or 4, as indicated). Unperturbed naive and activated samples (day 0 and 2) are included for reference (n = 3).

(B) Comparison of “opened” and “closed” ATAC-seq peak sets from day 6 to day 10 for each genotype.

(C) Visualization of opened and closed ATAC-seq peak sets, with selected nearest genes labeled.

(D) ATAC-seq signal tracks of selected gene loci. Representative replicates are shown for each condition.

(legend continued on next page)

loss of accessibility at exhaustion-induced AP-1 motif-containing regulatory elements, suggesting a similar mechanism in T cells. We envision that future work will build upon these findings to improve T cell function in the context of cancer immunotherapy.

STAR★METHODS

Detailed methods are provided in the online version of this paper and include the following:

- KEY RESOURCES TABLE
- RESOURCE AVAILABILITY
  - ○ Lead contact
  - ○ Materials availability
  - ○ Data and code availability
- EXPERIMENTAL MODEL AND SUBJECT DETAILS
  - ○ Mice
- METHOD DETAILS
  - ○ Primary murine T cell isolation and culture
  - ○ *In vitro* T cell exhaustion assay
  - ○ Measurement of cytokine production
  - ○ Growth curves
  - ○ *In vitro* killing assay
  - ○ B16-ovalbumin *in vivo* tumor models
  - ○ ATAC-seq sample processing
  - ○ Genome-wide sgRNA library
  - ○ sgRNA pool design and cloning
  - ○ Retrovirus production and transduction
  - ○ sgRNA library preparation and sequencing
  - ○ Tumor inoculation and T cell adoptive transfer for *in vivo* CRISPR experiments
  - ○ Tissue processing and isolation of tumor infiltrating lymphocytes
  - ○ Competition assay for validation of individual sgRNA proliferation
  - ○ Validation of Arid1a-targeting sgRNAs
  - ○ *In vitro* experiments in primary human T cells
  - ○ Pooled CRISPR screen in primary human T cells *in vivo*
  - ○ Direct-capture perturb-seq
- QUANTIFICATION AND STATISTICAL ANALYSIS
  - ○ Analysis summary
  - ○ ATAC-seq analysis
  - ○ Bulk sgRNA screening data analysis
  - ○ Comparison of CRISPR screen analytical methods
  - ○ GO term analysis
  - ○ Cytoscape interaction network
  - ○ Direct-capture perturb-seq analysis

SUPPLEMENTAL INFORMATION

Supplemental information can be found online at https://doi.org/10.1016/j.ccell.2022.06.001.

ACKNOWLEDGMENTS

We thank SciStories LLC for illustrations. This work was supported by National Institutes of Health grant no. U01CA260852 (to A.T.S.), the Burroughs Wellcome Fund Career Award for Medical Scientists (to A.T.S. and S.A.V.), the Parker Institute for Cancer Immunotherapy (to A.T.S.), a Pew-Stewart Scholars for Cancer Research Award (to A.T.S.), a Cancer Research Institute Technology Impact Award (to A.T.S.), a Baxter Foundation Faculty Scholar Award (to A.T.S.), and the Stanford Innovative Medicine Accelerator and Stanford ChEM-H (to A.T.S). A.M. has received the Burroughs Wellcome Fund Career Award for Medical Scientists and a Cancer Research Institute Lloyd J. Old STAR Award. The Marson lab has received support from the Parker Institute for Cancer Immunotherapy, the Innovative Genomics Institute, and the Chan Zuckerberg Biohub. J.A.B. was supported by a Stanford Graduate Fellowship and the National Science Foundation Graduate Research Fellowship under grant no. DGE-1656518. S.A.V. was supported by a Special Fellow Award from the Parker Institute for Cancer Immunotherapy and a Mentored Clinical Scientist Career Development Award from NCI/NIH (K08 CA237731).

AUTHOR CONTRIBUTIONS

J.A.B. and A.T.S. conceived the study. J.A.B., W.Y., N.L., Y.-T.C., Q.S., C.V.D., M.A.H., Z.M., and S.A.V. performed the experiments. K.A.F., E.S., N.K., and J.C. performed the experiments in primary human T cells. A.A., C.L.M., A.M., and J.C. provided resources and supervision for the experiments with primary human T cells. J.A.B. analyzed the data. K.E.Y. and B.D. assisted with the LCMV data. A.M.V. performed Western blot experiments. J.A.B. and A.T.S. supervised all of the experiments and wrote the manuscript. All of the authors reviewed and provided comments on the manuscript.

DECLARATION OF INTERESTS

A.T.S. is a scientific founder of Immunai and founder of Cartography Biosciences and receives research funding from Arsenal Biosciences, Allogene Therapeutics, and Merck Research Laboratories. J.A.B. is a consultant to Immunai. S.A.V. is an advisor to Immunai. K.E.Y. is a consultant to Cartography Biosciences. C.L.M. is a co-founder of Lyell Immunopharma and Syncopation Life Sciences, and consults for Lyell, Syncopation, NeoImmune Tech, Apricity, Nektar, Immatics, Mammoth, and Ensoma. A.A. is a co-founder of Tango Therapeutics, Azkarra Therapeutics, Ovibio Corporation, and Kytarro; a consultant for SPARC, Bluestar, Pro-Lynx, Earli, Cura, GenVivo, Ambagon, Phoenix Molecular Designs, and GlaxoSmithKline (GSK); a member of the Scientific Advisory Board of Genentech, GLAdiator, Circle and Cambridge Science Corporation; receives research support from SPARC and AstraZeneca; holds patents on the use of poly (ADP-ribose) polymerase (PARP) inhibitors held jointly with AstraZeneca. A.M. is a co-founder of Spotlight Therapeutics, Arsenal Biosciences, and Survey Genomics; a member of the Scientific Advisory Board of NewLimit; owns stock in Arsenal Biosciences, Spotlight Therapeutics, NewLimit, Survey Genomics, PACT Pharma, and Merck; has received fees from 23andMe, PACT Pharma, Juno Therapeutics, Trizell, Vertex, Merck, Amgen, Genentech, AlphaSights, Rupert Case Management, Bernstein, and ALDA; is an investor in and informal advisor to Offline Ventures; and is a client of EPIQ. The Marson lab has received research support from Juno Therapeutics, Epinomics, Sanofi, GSK, Gilead, and Anthem. K.A.F., E.S., J.C., A.A., A.M., and C.L.M. hold patents in the arena of CAR-T cell therapeutics. J.A.B. and A.T.S. have filed a patent related to the contents of this study.

Received: July 23, 2021
Revised: April 28, 2022
Accepted: June 1, 2022
Published: June 23, 2022

(E) Heatmap showing ATAC-seq coverage of each peak in the terminal exhaustion peak set for *Arid1a*-sgRNA and CTRL1 cells at days 6 and 10 in the *in vitro* exhaustion assay. Reference data from TILs is also included, as well as reference naive and activated cell profiles.

(F) chromVAR motif accessibility heatmap for *Arid1a*-sgRNA and CTRL1 ATAC-seq samples. Selected motifs are indicated on the right. Top 100 most variable motifs are shown.

See also Figure S8.

Please cite this article in press as: Belk et al., Genome-wide CRISPR screens of T cell exhaustion identify chromatin remodeling factors that limit T cell persistence, Cancer Cell (2022), https://doi.org/10.1016/j.ccell.2022.06.001

REFERENCES

Adamson, B., Norman, T.M., Jost, M., Cho, M.Y., Nuñez, J.K., Chen, Y., Villalta, J.E., Gilbert, L.A., Horlbeck, M.A., Hein, M.Y., et al. (2016). A multiplexed single-cell CRISPR screening Platform enables systematic dissection of the unfolded protein response. Cell *167*, 1867–1882.e21. https://doi.org/10.1016/j.cell.2016.11.048.

Alfei, F., Kanev, K., Hofmann, M., Wu, M., Ghoneim, H.E., Roelli, P., Utzschneider, D.T., von Hoesslin, M., Cullen, J.G., Fan, Y., et al. (2019). TOX reinforces the phenotype and longevity of exhausted T cells in chronic viral infection. Nature *571*, 265–269. https://doi.org/10.1038/s41586-019-1326-9.

Ataide, M.A., Komander, K., Knöpper, K., Peters, A.E., Wu, H., Eickhoff, S., Gogishvili, T., Weber, J., Grafen, A., Kallies, A., et al. (2020). BATF3 programs CD8+ T cell memory. Nat. Immunol. *21*, 1397–1407. https://doi.org/10.1038/s41590-020-0786-2.

Barber, D.L., Wherry, E.J., Masopust, D., Zhu, B., Allison, J.P., Sharpe, A.H., Freeman, G.J., and Ahmed, R. (2006). Restoring function in exhausted CD8 T cells during chronic viral infection. Nature *439*, 682–687. https://doi.org/10.1038/nature04444.

Belk, J.A., Daniel, B., and Satpathy, A.T. (2022). Epigenetic regulation of T cell exhaustion. Nat. Immunol. *23*, 848–860. https://doi.org/10.1038/s41590-022-01224-z.

Beltra, J.-C., Manne, S., Abdel-Hakeem, M.S., Kurachi, M., Giles, J.R., Chen, Z., Casella, V., Ngiow, S.F., Khan, O., Huang, Y.J., et al. (2020). Developmental relationships of four exhausted CD8+ T cell subsets reveals underlying transcriptional and epigenetic landscape control mechanisms. Immunity *52*, 825–841.e8. https://doi.org/10.1016/j.immuni.2020.04.014.

Chen, J., López-Moyado, I.F., Seo, H., Lio, C.-W.J., Hempleman, L.J., Sekiya, T., Yoshimura, A., Scott-Browne, J.P., and Rao, A. (2019). NR4A transcription factors limit CAR T cell function in solid tumours. Nature *567*, 530–534. https://doi.org/10.1038/s41586-019-0985-x.

Chen, S., Zhou, Y., Chen, Y., and Gu, J. (2018). fastp: an ultra-fast all-in-one FASTQ preprocessor. Bioinformatics *34*, i884–i890. https://doi.org/10.1093/bioinformatics/bty560.

Chen, Z., Arai, E., Khan, O., Zhang, Z., Ngiow, S.F., He, Y., Huang, H., Manne, S., Cao, Z., Baxter, A.E., et al. (2021). In vivo CD8+ T cell CRISPR screening reveals control by Fli1 in infection and cancer. Cell *184*, 1262–1280.e22. https://doi.org/10.1016/j.cell.2021.02.019.

Collier, J.L., Weiss, S.A., Pauken, K.E., Sen, D.R., and Sharpe, A.H. (2021). Not-so-opposite ends of the spectrum: CD8+ T cell dysfunction across chronic infection, cancer and autoimmunity. Nat. Immunol. *22*, 809–819. https://doi.org/10.1038/s41590-021-00949-7.

Corces, M.R., Trevino, A.E., Hamilton, E.G., Greenside, P.G., Sinnott-Armstrong, N.A., Vesuna, S., Satpathy, A.T., Rubin, A.J., Montine, K.S., Wu, B., et al. (2017). An improved ATAC-seq protocol reduces background and enables interrogation of frozen tissues. Nat. Methods *14*, 959–962. https://doi.org/10.1038/nmeth.4396.

Daniel, B., Yost, K.E., Sandor, K., Xia, Y., Qi, Y., Hiam-Galvez, K.J., Meier, S.L., Belk, J.A., Giles, J.R., Wherry, E.J., et al. (2021). Divergent clonal differentiation trajectories of T cell exhaustion. Preprint at bioRxiv. https://doi.org/10.1101/2021.12.16.472900.

DePeaux, K., and Delgoffe, G.M. (2021). Metabolic barriers to cancer immunotherapy. Nat. Rev. Immunol. *21*, 785–797. https://doi.org/10.1038/s41577-021-00541-y.

Dixit, A., Parnas, O., Li, B., Chen, J., Fulco, C.P., Jerby-Arnon, L., Marjanovic, N.D., Dionne, D., Burks, T., Raychowdhury, R., et al. (2016). Perturb-seq: dissecting molecular circuits with scalable single-cell RNA profiling of pooled genetic screens. Cell *167*, 1853–1866.e17. https://doi.org/10.1016/j.cell.2016.11.038.

Dong, M.B., Wang, G., Chow, R.D., Ye, L., Zhu, L., Dai, X., Park, J.J., Kim, H.R., Errami, Y., Guzman, C.D., et al. (2019). Systematic immunotherapy target discovery using genome-scale in vivo CRISPR screens in CD8 T cells. Cell *178*, 1189–1204.e23. https://doi.org/10.1016/j.cell.2019.07.044.

Flynn, R.A., Belk, J.A., Qi, Y., Yasumoto, Y., Wei, J., Alfajaro, M.M., Shi, Q., Mumbach, M.R., Limaye, A., DeWeirdt, P.C., et al. (2021). Discovery and functional interrogation of SARS-CoV-2 RNA-host protein interactions. Cell *184*, 2394–2411.e16. https://doi.org/10.1016/j.cell.2021.03.012.

Fraietta, J.A., Lacey, S.F., Orlando, E.J., Pruteanu-Malinici, I., Gohil, M., Lundh, S., Boesteanu, A.C., Wang, Y., O'Connor, R.S., Hwang, W.-T., et al. (2018a). Determinants of response and resistance to CD19 chimeric antigen receptor (CAR) T cell therapy of chronic lymphocytic leukemia. Nat. Med. *24*, 563–571. https://doi.org/10.1038/s41591-018-0010-1.

Fraietta, J.A., Nobles, C.L., Sammons, M.A., Lundh, S., Carty, S.A., Reich, T.J., Cogdill, A.P., Morrissette, J.J.D., DeNizio, J.E., Reddy, S., et al. (2018b). Disruption of TET2 promotes the therapeutic efficacy of CD19-targeted T cells. Nature *558*, 307–312. https://doi.org/10.1038/s41586-018-0178-z.

Gilbert, L.A., Horlbeck, M.A., Adamson, B., Villalta, J.E., Chen, Y., Whitehead, E.H., Guimaraes, C., Panning, B., Ploegh, H.L., Bassik, M.C., et al. (2014). Genome-scale CRISPR-mediated control of gene repression and activation. Cell *159*, 647–661. https://doi.org/10.1016/j.cell.2014.09.029.

Hao, Y., Hao, S., Andersen-Nissen, E., Mauck, W.M., Zheng, S., Butler, A., Lee, M.J., Wilk, A.J., Darby, C., Zager, M., et al. (2021). Integrated analysis of multimodal single-cell data. Cell *184*, 3573–3587.e29. https://doi.org/10.1016/j.cell.2021.04.048.

Hargreaves, D.C., and Crabtree, G.R. (2011). ATP-dependent chromatin remodeling: genetics, genomics and mechanisms. Cell Res. *21*, 396–420. https://doi.org/10.1038/cr.2011.32.

Henriksson, J., Chen, X., Gomes, T., Ullah, U., Meyer, K.B., Miragaia, R., Duddy, G., Pramanik, J., Yusa, K., Lahesmaa, R., and Teichmann, S.A. (2019). Genome-wide CRISPR screens in T helper cells reveal pervasive crosstalk between activation and differentiation. Cell *176*, 882–896.e18. https://doi.org/10.1016/j.cell.2018.11.044.

Huang, H., Zhou, P., Wei, J., Long, L., Shi, H., Dhungana, Y., Chapman, N.M., Fu, G., Saravia, J., Raynor, J.L., et al. (2021). In vivo CRISPR screening reveals nutrient signaling processes underpinning CD8+ T cell fate decisions. Cell *184*, 1245–1261.e21. https://doi.org/10.1016/j.cell.2021.02.021.

Khan, O., Giles, J.R., McDonald, S., Manne, S., Ngiow, S.F., Patel, K.P., Werner, M.T., Huang, A.C., Alexander, K.A., Wu, J.E., et al. (2019). TOX transcriptionally and epigenetically programs CD8 + T cell exhaustion. Nature *571*, 211–218. https://doi.org/10.1038/s41586-019-1325-x.

Kim, D., Paggi, J.M., Park, C., Bennett, C., and Salzberg, S.L. (2019). Graph-based genome alignment and genotyping with HISAT2 and HISAT-genotype. Nat. Biotechnol. *37*, 907–915. https://doi.org/10.1038/s41587-019-0201-4.

LaFleur, M.W., Nguyen, T.H., Coxe, M.A., Yates, K.B., Trombley, J.D., Weiss, S.A., Brown, F.D., Gillis, J.E., Coxe, D.J., Doench, J.G., et al. (2019). A CRISPR-Cas9 delivery system for in vivo screening of genes in the immune system. Nat. Commun. *10*, 1668. https://doi.org/10.1038/s41467-019-09656-2.

Li, W., Xu, H., Xiao, T., Cong, L., Love, M.I., Zhang, F., Irizarry, R.A., Liu, J.S., Brown, M., and Liu, X.S. (2014). MAGeCK enables robust identification of essential genes from genome-scale CRISPR/Cas9 knockout screens. Genome Biol. *15*, 554. https://doi.org/10.1186/s13059-014-0554-4.

Long, A.H., Haso, W.M., Shern, J.F., Wanhainen, K.M., Murgai, M., Ingaramo, M., Smith, J.P., Walker, A.J., Kohler, M.E., Venkateshwara, V.R., et al. (2015). 4-1BB costimulation ameliorates T cell exhaustion induced by tonic signaling of chimeric antigen receptors. Nat. Med. *21*, 581–590. https://doi.org/10.1038/nm.3838.

Love, M.I., Huber, W., and Anders, S. (2014). Moderated estimation of fold change and dispersion for RNA-seq data with DESeq2. Genome Biol. *15*, 550. https://doi.org/10.1186/s13059-014-0550-8.

Lynn, R.C., Weber, E.W., Sotillo, E., Gennert, D., Xu, P., Good, Z., Anbunathan, H., Lattin, J., Jones, R., Tieu, V., et al. (2019). c-Jun overexpression in CAR T cells induces exhaustion resistance. Nature *576*, 293–300. https://doi.org/10.1038/s41586-019-1805-z.

Mariathasan, S., Turley, S.J., Nickles, D., Castiglioni, A., Yuen, K., Wang, Y., Kadel, E.E., Iii, Koeppen, H., Astarita, J.L., Cubas, R., et al. (2018). TGFβ attenuates tumour response to PD-L1 blockade by contributing to exclusion of T cells. Nature *554*, 544–548. https://doi.org/10.1038/nature25501.

Please cite this article in press as: Belk et al., Genome-wide CRISPR screens of T cell exhaustion identify chromatin remodeling factors that limit T cell persistence, Cancer Cell (2022), https://doi.org/10.1016/j.ccell.2022.06.001

Mashtalir, N., D'Avino, A.R., Michel, B.C., Luo, J., Pan, J., Otto, J.E., Zullow, H.J., McKenzie, Z.M., Kubiak, R.L., St. Pierre, R., et al. (2018). Modular organization and assembly of SWI/SNF family chromatin remodeling complexes. Cell *175*, 1272–1288.e20. https://doi.org/10.1016/j.cell.2018.09.032.

Mathur, R., Alver, B.H., San Roman, A.K., Wilson, B.G., Wang, X., Agoston, A.T., Park, P.J., Shivdasani, R.A., and Roberts, C.W.M. (2017). ARID1A loss impairs enhancer-mediated gene regulation and drives colon cancer in mice. Nat. Genet. *49*, 296–302. https://doi.org/10.1038/ng.3744.

McKinney, E.F., Lee, J.C., Jayne, D.R.W., Lyons, P.A., and Smith, K.G.C. (2015). T-cell exhaustion, co-stimulation and clinical outcome in autoimmunity and infection. Nature *523*, 612–616. https://doi.org/10.1038/nature14468.

McLane, L.M., Abdel-Hakeem, M.S., and Wherry, E.J. (2019). CD8 T cell exhaustion during chronic viral infection and cancer. Annu. Rev. Immunol. *37*, 457–495. https://doi.org/10.1146/annurev-immunol-041015-055318.

Miller, B.C., Sen, D.R., Al Abosy, R., Bi, K., Virkud, Y.V., LaFleur, M.W., Yates, K.B., Lako, A., Felt, K., Naik, G.S., et al. (2019). Subsets of exhausted CD8 + T cells differentially mediate tumor control and respond to checkpoint blockade. Nat. Immunol. *20*, 326–336. https://doi.org/10.1038/s41590-019-0312-6.

Morgens, D.W., Deans, R.M., Li, A., and Bassik, M.C. (2016). Systematic comparison of CRISPR-Cas9 and RNAi screens for essential genes. Nat. Biotechnol. *34*, 634–636. https://doi.org/10.1038/nbt.3567.

Odorizzi, P.M., Pauken, K.E., Paley, M.A., Sharpe, A., and Wherry, E.J. (2015). Genetic absence of PD-1 promotes accumulation of terminally differentiated exhausted CD8+ T cells. J. Exp. Med. *212*, 1125–1137. https://doi.org/10.1084/jem.20142237.

Paley, M.A., Kroy, D.C., Odorizzi, P.M., Johnnidis, J.B., Dolfi, D.V., Barnett, B.E., Bikoff, E.K., Robertson, E.J., Lauer, G.M., Reiner, S.L., and Wherry, E.J. (2012). Progenitor and terminal subsets of CD8+ T cells cooperate to contain chronic viral infection. Science *338*, 1220–1225. https://doi.org/10.1126/science.1229620.

Parnas, O., Jovanovic, M., Eisenhaure, T.M., Herbst, R.H., Dixit, A., Ye, C.J., Przybylski, D., Platt, R.J., Tirosh, I., Sanjana, N.E., et al. (2015). A genome-wide CRISPR screen in primary immune cells to dissect regulatory networks. Cell *162*, 675–686. https://doi.org/10.1016/j.cell.2015.06.059.

Pauken, K.E., Sammons, M.A., Odorizzi, P.M., Manne, S., Godec, J., Khan, O., Drake, A.M., Chen, Z., Sen, D.R., Kurachi, M., et al. (2016). Epigenetic stability of exhausted T cells limits durability of reinvigoration by PD-1 blockade. Science *354*, 1160–1165. https://doi.org/10.1126/science.aaf2807.

Philip, M., Fairchild, L., Sun, L., Horste, E.L., Camara, S., Shakiba, M., Scott, A.C., Viale, A., Lauer, P., Merghoub, T., et al. (2017). Chromatin states define tumour-specific T cell dysfunction and reprogramming. Nature *545*, 452–456. https://doi.org/10.1038/nature22367.

Platt, R.J., Chen, S., Zhou, Y., Yim, M.J., Swiech, L., Kempton, H.R., Dahlman, J.E., Parnas, O., Eisenhaure, T.M., Jovanovic, M., et al. (2014). CRISPR-Cas9 knockin mice for genome editing and cancer modeling. Cell *159*, 440–455. https://doi.org/10.1016/j.cell.2014.09.014.

Pritykin, Y., van der Veeken, J., Pine, A.R., Zhong, Y., Sahin, M., Mazutis, L., Pe'er, D., Rudensky, A.Y., and Leslie, C.S. (2021). A unified atlas of CD8 T cell dysfunctional states in cancer and infection. Mol. Cell *81*, 2477–2493.e10. https://doi.org/10.1016/j.molcel.2021.03.045.

Raju, S., Xia, Y., Daniel, B., Yost, K.E., Bradshaw, E., Tonc, E., Verbaro, D.J., Kometani, K., Yokoyama, W.M., Kurosaki, T., et al. (2021). Identification of a T-bethi quiescent exhausted CD8 T cell subpopulation that can differentiate into TIM3+CX3CR1+ effectors and memory-like cells. J. Immunol. *206*, 2924–2936. https://doi.org/10.4049/jimmunol.2001348.

Replogle, J.M., Norman, T.M., Xu, A., Hussmann, J.A., Chen, J., Cogan, J.Z., Meer, E.J., Terry, J.M., Riordan, D.P., Srinivas, N., et al. (2020). Combinatorial single-cell CRISPR screens by direct guide RNA capture and targeted sequencing. Nat. Biotechnol. *38*, 954–961. https://doi.org/10.1038/s41587-020-0470-y.

Ribas, A., and Wolchok, J.D. (2018). Cancer immunotherapy using checkpoint blockade. Science *359*, 1350–1355. https://doi.org/10.1126/science.aar4060.

Roth, T.L., Li, P.J., Blaeschke, F., Nies, J.F., Apathy, R., Mowery, C., Yu, R., Nguyen, M.L.T., Lee, Y., Truong, A., et al. (2020). Pooled knockin targeting for genome engineering of cellular immunotherapies. Cell *181*, 728–744.e21. https://doi.org/10.1016/j.cell.2020.03.039.

Sakuishi, K., Apetoh, L., Sullivan, J.M., Blazar, B.R., Kuchroo, V.K., and Anderson, A.C. (2010). Targeting Tim-3 and PD-1 pathways to reverse T cell exhaustion and restore anti-tumor immunity. J. Exp. Med. *207*, 2187–2194. https://doi.org/10.1084/jem.20100643.

Satpathy, A.T., Granja, J.M., Yost, K.E., Qi, Y., Meschi, F., McDermott, G.P., Olsen, B.N., Mumbach, M.R., Pierce, S.E., Corces, M.R., et al. (2019). Massively parallel single-cell chromatin landscapes of human immune cell development and intratumoral T cell exhaustion. Nat. Biotechnol. *37*, 925–936. https://doi.org/10.1038/s41587-019-0206-z.

Schep, A.N., Wu, B., Buenrostro, J.D., and Greenleaf, W.J. (2017). chromVAR: inferring transcription-factor-associated accessibility from single-cell epigenomic data. Nat. Methods *14*, 975–978. https://doi.org/10.1038/nmeth.4401.

Schietinger, A., Philip, M., Krisnawan, V.E., Chiu, E.Y., Delrow, J.J., Basom, R.S., Lauer, P., Brockstedt, D.G., Knoblaugh, S.E., Hämmerling, G.J., et al. (2016). Tumor-specific T cell dysfunction is a dynamic antigen-driven differentiation program initiated early during tumorigenesis. Immunity *45*, 389–401. https://doi.org/10.1016/j.immuni.2016.07.011.

Scott, A.C., Dündar, F., Zumbo, P., Chandran, S.S., Klebanoff, C.A., Shakiba, M., Trivedi, P., Menocal, L., Appleby, H., Camara, S., et al. (2019). TOX is a critical regulator of tumour-specific T cell differentiation. Nature *571*, 270–274. https://doi.org/10.1038/s41586-019-1324-y.

Scott-Browne, J.P., López-Moyado, I.F., Trifari, S., Wong, V., Chavez, L., Rao, A., and Pereira, R.M. (2016). Dynamic changes in chromatin accessibility occur in CD8+ T cells responding to viral infection. Immunity *45*, 1327–1340. https://doi.org/10.1016/j.immuni.2016.10.028.

Sen, D.R., Kaminski, J., Barnitz, R.A., Kurachi, M., Gerdemann, U., Yates, K.B., Tsao, H.-W., Godec, J., LaFleur, M.W., Brown, F.D., et al. (2016). The epigenetic landscape of T cell exhaustion. Science *354*, 1165–1169. https://doi.org/10.1126/science.aae0491.

Seo, H., González-Avalos, E., Zhang, W., Ramchandani, P., Yang, C., Lio, C.-W.J., Rao, A., and Hogan, P.G. (2021). BATF and IRF4 cooperate to counter exhaustion in tumor-infiltrating CAR T cells. Nat. Immunol. *22*, 983–995. https://doi.org/10.1038/s41590-021-00964-8.

Shalem, O., Sanjana, N.E., Hartenian, E., Shi, X., Scott, D.A., Mikkelsen, T.S., Heckl, D., Ebert, B.L., Root, D.E., Doench, J.G., and Zhang, F. (2014). Genome-scale CRISPR-Cas9 knockout screening in human cells. Science *343*, 84–87. https://doi.org/10.1126/science.1247005.

Shannon, P., Markiel, A., Ozier, O., Baliga, N.S., Wang, J.T., Ramage, D., Amin, N., Schwikowski, B., and Ideker, T. (2003). Cytoscape: a software environment for integrated models of biomolecular interaction networks. Genome Res. *13*, 2498–2504. https://doi.org/10.1101/gr.1239303.

Shifrut, E., Carnevale, J., Tobin, V., Roth, T.L., Woo, J.M., Bui, C.T., Li, P.J., Diolaiti, M.E., Ashworth, A., and Marson, A. (2018). Genome-wide CRISPR screens in primary human T cells reveal key regulators of immune function. Cell *175*, 1958–1971.e15. https://doi.org/10.1016/j.cell.2018.10.024.

Singer, M., Wang, C., Cong, L., Marjanovic, N.D., Kowalczyk, M.S., Zhang, H., Nyman, J., Sakuishi, K., Kurtulus, S., Gennert, D., et al. (2016). A distinct gene module for dysfunction uncoupled from activation in tumor-infiltrating T cells. Cell *166*, 1500–1511.e9. https://doi.org/10.1016/j.cell.2016.08.052.

Spitzer, M.H., Carmi, Y., Reticker-Flynn, N.E., Kwek, S.S., Madhireddy, D., Martins, M.M., Gherardini, P.F., Prestwood, T.R., Chabon, J., Bendall, S.C., et al. (2017). Systemic immunity is required for effective cancer immunotherapy. Cell *168*, 487–502.e15. https://doi.org/10.1016/j.cell.2016.12.022.

Szklarczyk, D., Gable, A.L., Lyon, D., Junge, A., Wyder, S., Huerta-Cepas, J., Simonovic, M., Doncheva, N.T., Morris, J.H., Bork, P., et al. (2019). STRING v11: protein-protein association networks with increased coverage, supporting functional discovery in genome-wide experimental datasets. Nucleic Acids Res. *47*, D607–D613. https://doi.org/10.1093/nar/gky1131.

Vardhana, S.A., Hwee, M.A., Berisa, M., Wells, D.K., Yost, K.E., King, B., Smith, M., Herrera, P.S., Chang, H.Y., Satpathy, A.T., et al. (2020). Impaired mitochondrial oxidative phosphorylation limits the self-renewal of T cells exposed to persistent antigen. Nat. Immunol. *21*, 1022–1033. https://doi.org/10.1038/s41590-020-0725-2.

Vierbuchen, T., Ling, E., Cowley, C.J., Couch, C.H., Wang, X., Harmin, D.A., Roberts, C.W.M., and Greenberg, M.E. (2017). AP-1 transcription factors and the BAF complex mediate signal-dependent enhancer selection. Mol. Cell *68*, 1067–1082.e12. https://doi.org/10.1016/j.molcel.2017.11.026.

Wang, T., Wei, J.J., Sabatini, D.M., and Lander, E.S. (2014). Genetic screens in human cells using the CRISPR-Cas9 system. Science *343*, 80–84. https://doi.org/10.1126/science.1246981.

Weber, E.W., Parker, K.R., Sotillo, E., Lynn, R.C., Anbunathan, H., Lattin, J., Good, Z., Belk, J.A., Daniel, B., Klysz, D., et al. (2021). Transient rest restores functionality in exhausted CAR-T cells through epigenetic remodeling. Science *372*, eaba1786. https://doi.org/10.1126/science.aba1786.

Wei, J., Long, L., Zheng, W., Dhungana, Y., Lim, S.A., Guy, C., Wang, Y., Wang, Y.-D., Qian, C., Xu, B., et al. (2019). Targeting REGNASE-1 programs long-lived effector T cells for cancer therapy. Nature *576*, 471–476. https://doi.org/10.1038/s41586-019-1821-z.

Wherry, E.J., and Kurachi, M. (2015). Molecular and cellular insights into T cell exhaustion. Nat. Rev. Immunol. *15*, 486–499. https://doi.org/10.1038/nri3862.

Xu, G., Chhangawala, S., Cocco, E., Razavi, P., Cai, Y., Otto, J.E., Ferrando, L., Selenica, P., Ladewig, E., Chan, C., et al. (2020). ARID1A determines luminal identity and therapeutic response in estrogen-receptor-positive breast cancer. Nat. Genet. *52*, 198–207. https://doi.org/10.1038/s41588-019-0554-0.

Yost, K.E., Chang, H.Y., and Satpathy, A.T. (2021). Recruiting T cells in cancer immunotherapy. Science *372*, 130–131. https://doi.org/10.1126/science.abd1329.

Yost, K.E., Satpathy, A.T., Wells, D.K., Qi, Y., Wang, C., Kageyama, R., McNamara, K.L., Granja, J.M., Sarin, K.Y., Brown, R.A., et al. (2019). Clonal replacement of tumor-specific T cells following PD-1 blockade. Nat. Med. *25*, 1251–1259. https://doi.org/10.1038/s41591-019-0522-3.

Zajac, A.J., Blattman, J.N., Murali-Krishna, K., Sourdive, D.J., Suresh, M., Altman, J.D., and Ahmed, R. (1998). Viral immune evasion due to persistence of activated T cells without effector function. J. Exp. Med. *188*, 2205–2213. https://doi.org/10.1084/jem.188.12.2205.

Zhang, Y., Liu, T., Meyer, C.A., Eeckhoute, J., Johnson, D.S., Bernstein, B.E., Nusbaum, C., Myers, R.M., Brown, M., Li, W., and Liu, X.S. (2008). Model-based analysis of ChIP-seq (MACS). Genome Biol. *9*, R137. https://doi.org/10.1186/gb-2008-9-9-r137.

STAR★METHODS

KEY RESOURCES TABLE

REAGENT or RESOURCE	SOURCE	IDENTIFIER
Antibodies		
Ultra-LEAF Purified anti-mouse CD3ε Antibody (clone: 145-2C11)	Biolegend	Cat#100340; RRID: AB_11149115
Ultra-LEAF(TM) Purified anti-mouse CD28 Antibody (clone: 37.51)	Biolegend	Cat#102116; RRID: AB_11147170
PerCP Cy5.5 anti-mouse CD8 Antibody (clone: 53–6.7)	Biolegend	Cat#100734; RRID: AB_2075239
PE/Cyanine7 anti-mouse CD279 (PD-1) antibody (clone: RMP1-30)	Biolegend	Cat# 109110, RRID: AB_572017
PE anti-mouse CD366 (Tim-3) antibody (clone: RMT3-23)	Biolegend	Cat# 119704, RRID: AB_345378
PE/Cyanine7 anti-mouse CD3 antibody (clone: 17A2)	Biolegend	Cat# 100220, RRID: AB_1732057
APC/Cyanine7 anti-mouse CD45 antibody (clone: 30-F11)	Biolegend	Cat# 103116, RRID: AB_312981
Chemicals, peptides, and recombinant proteins		
Recombinant Mouse IL-2 Protein	R&D system	Cat# 402-ML-020
RPMI 1640 Medium	GIBCO	Cat#11995073
Penicillin-Streptomycin (10,000 U/mL)	GIBCO	Cat#15140122
2-Mercaptoethanol	Sigma Aldrich	Cat#M6250-10ML
LIVE/DEAD™ Fixable Green Dead Cell Stain Kit, for 488 nm excitation	Invitrogen	Cat#L23101
Critical commercial assays		
CD8a+ T Cell Isolation Kit, mouse	Miltenyi	Cat# 130-104-075
Mitenyi tumor Dissociation Kit	Miltenyi	Cat# 130-096-730
EasySep™ Mouse CD8a Positive Selection Kit II	Stemcell	Cat# 18953
Deposited data		
Mouse and human ATAC-seq	This paper	GEO: GSE203591
In vivo Perturb-seq	This paper	GEO: GSE203592
Experimental models: Cell lines		
B16-F10	ATCC	Cat# CRL-6475
A-375	ATCC	Cat# CRL-1619
MC-38	Stanford Tumor Core	N/A
Experimental models: Organisms/strains		
Rosa26-Cas9 knockin mice	Jackson Labs	Cat# 026179
OT-1 mice	Jackson Labs	Cat# 003831
Rag1$^{-/-}$ mice	Jackson Labs	Cat# 002216
C57BL/6J mice	Jackson Labs	Cat# 000664
Recombinant DNA		
pMSCV-U6sgRNA(BbsI)-PGKpuro2ABFP	Addgene	Cat# 102796
Teichmann Retroviral Mouse Genome-wide CRISPR Knockout Library	Addgene	Cat# 104861
Custom sgRNA mini-pools detailed in Table S2.	N/A	N/A
Software and algorithms		
Seurat		
HISAT2	(Kim et al., 2019)	http://daehwankimlab.github.io/hisat2/
cellranger	10X Genomics	https://support.10xgenomics.com/single-cell-gene-expression/software/pipelines/latest/using/count
Seurat	(Hao et al., 2021)	https://satijalab.org/seurat/index.html

Please cite this article in press as: Belk et al., Genome-wide CRISPR screens of T cell exhaustion identify chromatin remodeling factors that limit T cell persistence, Cancer Cell (2022), https://doi.org/10.1016/j.ccell.2022.06.001

RESOURCE AVAILABILITY

Lead contact

Further information and requests for resources and reagents should be directed to and will be fulfilled by the lead contact, Ansuman Satpathy (satpathy@stanford.edu).

Materials availability

CRISPR sgRNA mini-pool plasmids generated in this study are available from the lead contact upon request.

Data and code availability

CRISPR screen counts tables and z-score tables are available with the manuscript as supplemental data. ATAC-seq and Perturb-seq data are available on GEO under accession GSE203593. Scripts used to analyze CRISPR screen data have been previously open-sourced and are available at: https://github.com/juliabelk/sarscov2_chirp_ms.

EXPERIMENTAL MODEL AND SUBJECT DETAILS

Mice

Wild type mice were C57BL/6J mice (JAX: 000664). Rosa26-Cas9 knockin mice were bred in house (JAX: 026179). OT-1 mice (JAX: 003831) were crossed with Cas9 mice and then bred in-house. Rag1$^{-/-}$ mice were bred in-house (JAX: 002216). C57BL/6 Scid mice (JAX: 001913) and NSG mice (JAX: 005557) were procured from JAX. All animal studies were performed in accordance with the Stanford University Institutional Animal Care and Use Committee under protocol APLAC-33814. All studies were performed in animals between 8 and 12 weeks of age.

METHOD DETAILS

Primary murine T cell isolation and culture

Spleens were collected and mashed through a 70 μM filter. Red blood cells were lysed with ACK lysis buffer (Gibco) and incubated for 6 min before washing with PBS. Cells were counted and then resuspended in MACS buffer (PBS + 0.5% BSA + 2 μM EDTA). CD8 T cells were enriched using the mouse CD8$^+$ T cells isolation kit from Miltenyi (Miltenyi Cat# 130-104-075) and then resuspended in RPMI with 10% FBS, 1% Sodium pyruvate, 1% Non-essential amino-acids, 100U Pen/Strep, 50 nM of B-mercaptoethanol (cRPMI) and supplemented with 10 ng/mL of mouse IL-2. Cells were seeded at a concentration of 1 million cells/ml on plates coated with 5 ug/ml of anti-CD3 and 2 μg/mL of anti-CD28. Cells were kept on these activation plates for 48 h at the beginning of all experiments. CD8$^+$ T cell purity was verified via flow cytometry. Cells were passaged every two days and maintained at 1 million cells/mL.

In vitro T cell exhaustion assay

To induce T cell exhaustion, chronic stimulation was performed using plates coated with anti-CD3 at 5 μg/mL (in the continued presence of 10 ng/mL IL-2). Cells were passaged onto a fresh coated plate every two days and analyzed on Day 6, 8, or 10 as described in the Results. In contrast, acutely stimulated cells were maintained in 10 ng/mL IL-2 alone, passaged every two days, and analyzed on Day 6, 8, or 10, as described in the Results.

Measurement of cytokine production

T cells were re-stimulated with phorbol myristate acetate (Sigma, 50 ng/mL) and ionomycin (Sigma, 500 ng/mL) or plate bound anti-CD3 at 3 μg/mL. After 90 min, cells were treated with brefeldin A to block cytokine secretion. Then, 3 h later, cells were stained for surface markers and simultaneously labeled with Live/Dead Blue Viability Dye (Thermo Fisher) for 20 min at 4°C. Cells were washed twice and fixed overnight using a FoxP3 Fixation/Permeabilization Kit (Thermo Fisher). The next day, cells were washed and stained for intracellular cytokines for 1 h at room temperature. They were then washed three times and analyzed using an LSR Fortessa machine (Beckman Dickinson). FlowJo v.10.0 was used for data analysis. All experiments were performed with at least two biological replicates. Antibodies used (at 1:100 unless otherwise noted) were TNF-PE (BioLegend, MP6-XT22, 506306), PD-1-PECy7 (BioLegend, RMP1–30, 109110) IFN-γ-FITC (BioLegend, XMG1.2, 505806), CD4-BV711 (BioLegend, RM4–5, 100550), and CD8α-BV786 (BioLegend, 53–6.7, 100750).

Growth curves

After activation (described above), T cells were plated in 24-well plates at 5 × 10^5 cells in 1 mL of RPMI-1640 medium containing 10% FBS, 2 mM l-glutamine, 5 μM β-ME and 10 ng/mL IL-2, and with (chronic) or without (acute) plate-bound anti-CD3. Every 2 days throughout the experiment, cells were collected and counted using a Beckmann Coulter Counter with a cell volume gate of 75–4,000 femtoliters. Then, 50% of the cells were re-plated in 1 mL of fresh T cell medium. All experiments were performed at least two independent times.

Please cite this article in press as: Belk et al., Genome-wide CRISPR screens of T cell exhaustion identify chromatin remodeling factors that limit T cell persistence, Cancer Cell (2022), https://doi.org/10.1016/j.ccell.2022.06.001

In vitro killing assay

B16 cells expressing a Luciferase reporter were pulsed with SIINFEKL peptide (Invivogen) at the concentrations noted in Figure S1 for 4 h at 37C. They were then washed twice and plated at 4 x 10^4 cells per well along with 1 × 10^5 OT-1 transgenic T cells that had been acutely or chronically stimulated for 8 days as previously described. After 24 h of co-culture, cells were lysed and luciferase activity was measured using a Luciferase Assay Kit (Promega), following manufacturer's instructions. Luciferase activity was normalized to cells cultured in the absence of T cells.

B16-ovalbumin *in vivo* tumor models

C57BL/6 scid (Jackson 001913) mice were injected subcutaneously with 2 × 10^5 B16-OVA cells in a 1:1 mix of PBS and Matrigel (Corning). 5 days later, 2 × 10^6 OT-1 T cells that had been acutely or chronically stimulated as described previously were adoptively transferred to mice via retro-orbital injection. Mice were monitored once per day and were euthanized for signs of morbidity.

ATAC-seq sample processing

ATAC-seq was performed using the Omni-ATAC protocol (Corces et al., 2017). Briefly, 50,000 live cells were purified by flow cytometry immediately prior to ATAC-seq. Lysis, nuclei isolation, and transposition were performed according to the Omni-ATAC protocol. Libraries were prepared for sequencing and sequenced in 2x75 dual-indexed format on an Illumina NovaSeq.

Genome-wide sgRNA library

Retroviral Mouse Genome-wide CRISPR Knockout Library was a gift from Sarah Teichmann (Addgene #104861). The library was amplified via electroporation and confirmed by sequencing.

sgRNA pool design and cloning

The sgRNA mini-pool was designed using our previously developed protocol for cloning into a lentiviral backbone and then subcloned into retroviral construct pMSCV (Flynn et al., 2021). The lentiCRISPR-v2 was a gift from Feng Zhang (Addgene plasmid #52961). pMSCV-U6sgRNA(BbsI)-PGKpuro2ABFP was a gift from Sarah Teichmann (Addgene plasmid #102796).

The mini-pool targeting 300 top hits included 2,000 sgRNAs, with 6 sgRNAs per gene as well as 100 non-targeting and 100 single-targeting controls. Briefly, six 20bp variable sgRNA sequences per target gene were obtained from the Broad Genetic Perturbation Platform (GPP) genome wide designs: sgRNA_design_10090_GRCm38_SpyoCas9_CRISPRko_NCBI_20200317.txt.gz, available online at https://portals.broadinstitute.org/gpp/public/dir?dirpath=sgrna_design. 100 non-targeting and 100 single-targeting negative control guides designed for the mouse genome, also from the Broad GPP web portal, were included. The single-targeting sequences are designed to match exactly one intergenic location in the reference genome. A "G" was added to the start of each 20bp sequence. This 21bp sequence was flanked by BsmBI-v2 enzyme sites and then two nested PCR handles. Pooled oligos were synthesized by Twist Bioscience. Oligos were amplified by two rounds of PCR and the lentiCRISPR-v2 backbone was digested overnight with Esp3I. One step digestion/ligation of amplified oligos into lentiCRISPR-v2 was performed at 37C for 1 h in a 20 uL reaction with 1 uL T4 ligase, 1 uL Esp3I, 2 uL T4 ligase buffer, 200 ng digested backbone, and 50 ng amplified insert. Reaction was heat inactivated for 15 min at 65C and then 1 uL was electroporated using 25 uL Lucigen Endura electrocompetent cells and a BioRad MicroPulser with 0.1 cm gap cuvettes. After 1 h recovery in SOC, a 1000x dilution was plated onto an agar plate to confirm library coverage. The remainder was cultured overnight in a 150 mL liquid culture and then purified by maxiprep. Finally, the pool was subcloned into pMSCV by Gibson Assembly of the sgRNA variable region amplified via PCR and pMSCV backbone pre-digested with BbsI. Electroporation was repeated as described above. Guide representation was confirmed by sequencing.

The sgRNA SWI/SNF mini-pool and micro-pool for Perturb-seq were designed with 4 guides per gene, as described above for the mini-pool using the Broad GPP mouse genome-wide designs. The SWI/SNF mini-pool contained 50 single-targeting controls and Perturb-seq micro-pool contained 12 single-targeting controls. Two primers were ordered per designed guide, for cloning via annealing. The pMSCV vector was digested with BbsI. All primer pairs were annealed separately. Annealed products were pooled, diluted, and then ligated into pMSCV. Amplification was performed using Stbl3 Chemically Competent cells (ThermoFisher C737303) and library coverage was confirmed via colony counting and then sequencing.

Retrovirus production and transduction

The pMSCV plasmid was transfected into GP2-293 cells (Takara, RetroPack™ PT67 Cell Line) or 293T HEK cells at roughly 80% confluency in 15 cm tissue culture plates coated with poly-d-lysine. Viral supernatant was collected at 48 and 72h post-transfection, filtered via a 0.45 μm filtration unit (Millipore). Filtered virus was concentrated using the LentiX concentrator (Takara) at 1500 x g for 45 min. The concentrated supernatant was subsequently aliquoted, flash frozen, and stored in −80°C until use.

$CD8^+$ T cells were transduced with concentrated retrovirus 24 h after isolation. 4 μg/mL of polybrene was added to each well. Plates were sealed and then spun at 1100x g at 32C for 90 min. 24 h after spinfection (ie, starting on day 2) cells were checked for fluorescence via flow cytometry and 2 μg/mL puromycin was added to the media.

sgRNA library preparation and sequencing

For samples from *in vitro* chronic culture, live cells were first isolated via FACS. gDNA was extracted using a commercially available kit (Zymo Cat# D3025). sgRNA libraries were prepared for sequencing as previously described (Flynn et al., 2021). Briefly, a standard three-step amplification protocol was used. First, sgRNAs were amplified off of gDNA using primers specific to the pMSCV vector for 22 cycles of PCR. 100 uL reactions with up to 4 μg of gDNA per reaction were used, and the number of reactions was scaled up until all gDNA was used. For sequencing of plasmid pools, this first PCR was skipped. For the second PCR, a 0-7bp offset was added to the front of the library using 8 pooled stagger primers to increase the diversity of the library. PCR2 primer target sites were nested inside those of PCR1 to improve the specificity of the product. Finally, in PCR3, index sequences were added. Libraries were sequenced in dual-indexed 1x75 bp or 1x150 bp format on either an Illumina NextSeq or NovaSeq.

Tumor inoculation and T cell adoptive transfer for *in vivo* CRISPR experiments

MC-38 or B16 cells ectopically expressing an mCherry-ovalbumin fusion construct were prepared for injection by resuspending in a 1:1 mixture of matrigel and PBS. 10^6 cells per tumor were injected subcutaneously into the flanks of Rag1$^{-/-}$ mice (two tumors per mouse). Tumors were measured every three days. Cas9/OT-1 CD8$^+$ T cells were transduced with sgRNA pools or individual sgRNAs and selected with puromycin for 4 days, as described above. T cells were then intravenously injected into tumor-bearing mice on day 6. For *in vivo* competition assays, cells were mixed immediately prior to injection. 9 days after T cell injection, the spleen and tumors were harvested from each mouse.

Tissue processing and isolation of tumor infiltrating lymphocytes

Tumors were weighed and then minced into small pieces. The tumors were transferred to a gentleMACS C tube and digested in the protocol-recommended enzyme mix with a gentleMACS octo dissociator using the soft/medium tumor program. Tumor suspensions were then filtered with a 70 μM filter and then subject to RBC lysis. Spleens were mashed and filtered through a 70 μM strainer, then treated with RBC lysis buffer. For bulk sgRNA sequencing and Perturb-seq, T cells were isolated from the tumors and/or spleens by FACS. Samples were washed twice with MACS buffer and stained for 30 min on ice. CD8$^+$ BFP$^+$ cells were isolated via flow cytometry.

Competition assay for validation of individual sgRNA proliferation

The pMSCV retroviral vector was modified to replace the BFP-puromycin fusion with a VEX-puromycin fusion (pMSCV-VEX). CTRL1 sgRNA was cloned into pMSCV-VEX, while two *Arid1a*-sgRNA sgRNAs (*Arid1a*-1 and *Arid1a*-2) were cloned into pMSCV. Cells were separately transduced with either vector, selected with puromycin to enrich for transduced cells, mixed together, and then subjected to either the *in vitro* exhaustion assay or injected into tumor bearing mice. Individual guides were cloned by annealing pairs of primers, as described above. The *Arid1a*-1 sgRNA sequence used was GCAGCTGCGAAGATATCGGG and the *Arid1a*-2 sequence used was CAGCAGAACTCGCACGACCA. The CTRL sgRNA sequence used was CTTACTCGACGAATGAGCCC. Tumor processing was performed as described above for the *in vivo* validation.

Validation of Arid1a-targeting sgRNAs

Tracking of indels by decomposition (TIDE): Genomic DNA was isolated from transduced cells using a commercially available kit (Zymo Cat# D3025). PCR reactions were performed with primers surrounding the expected edit site and 50 ng of input DNA. PCR conditions were 30 s at 98C, followed by 10 s at 98C, 10 s annealing at 60C, 25 s at 72C for 35 cycles, then 2 min at 72C. The PCR amplicons were purified with a commercially available Zymo DNA clean up kit and sanger sequenced. Quantification of edits was performed using the online tool https://tide.nki.nl/.

Western blot: Protein lysates were prepared from mouse T cells transduced with the indicated sgRNA using a radioimmunoprecipitation assay (RIPA) buffer system (Santa Cruz, sc-24948). Protein concentrations were quantified using the bicinchoninic Acid (BCA) assay (Pierce, ThermoFisher 23225). 20 μg of protein per sample was loaded and run on a 4–12% Bis-Tris PAGE gel (NuPAGE 4–12% Bis-Tris Protein Gel, Invitrogen) and transferred onto a polyvinylidene fluoride (PVDF) membrane (Immobilon-FL, EMD Millipore). After blocking membranes for 1 h with 5% milk in PBST at room temperature (RT), membranes were incubated overnight at 4°C with primary antibodies against Arid1a (rabbit, 1:1000, Cell Signaling, 12354S: Lot 4), Arid1b (mouse, 1:1000, Abcam, ab57461: Lot GR3345290-4), Smarca4 (rabbit, 1:1000, Cell Signaling, 49360S: Lot 3) and Tbp (mouse, Abcam, ab51841: Lot GR3313213-3). The next day, PBST was used to wash membranes three times. Next, membranes were incubated for 1 h at RT with species-specific secondary antibodies conjugated to near-infrared fluorophores: Goat Anti-Mouse IgG Polyclonal Antibody (IRDye 680RD, 1:10,000, LI-COR Biosciences, 926–68070) or Goat Anti-Rabbit IgG Polyclonal Antibody (IRDye 800CW, 1:10,000, LI-COR Biosciences, 926–32211). After secondary antibody application, PBST was used to wash membranes three times, and then membranes were imaged using a LI-COR Odyssey CLx imaging system (LI-COR). Protein band intensities were quantified using Image Studio Lite (LI-COR) with built-in background correction and normalization to Tbp controls. Statistical analysis comparing Arid1a levels normalized to Tbp was performed using Dunnett's multiple comparisons test on Prism (v9.2.0).

In vitro experiments in primary human T cells

T cell expansion and viability assays: T cells were activated for 4 days at a 1:3 ratio of T cells to anti-CD3/28 Dynabeads (Invitrogen). T cell expansion assays were performed with IL-2 in the culture medium at 10 ng/mL. Cell counts and viability measurements were obtained using the Cellaca Mx Automated Cell Counter (Nexcelom). Cells were stained with acridine orange and propidium iodide to assess viability.

Targeted CRISPR gene editing: Ribonucleoprotein (RNP) was preparing using synthetic sgRNA with 2'-O-methyl phosphorothioate modification (Synthego) diluted in TE buffer at 100 μM. 5 μL sgRNA was incubated with 2.5 μL Duplex Buffer (IDT) and 2.5 μg Alt-R S.p. Cas9 Nuclease V3 (IDT) for 30 min at room temperature. 100 μL reactions were assembled with 10 million T cells, 90 μL P3 buffer (Lonza), and 10 μL RNP. Cell were pulsed with protocol EO115 using the P3 Primary Cell 4D-Nucleofector Kit and 4D Nucleofector System (Lonza). Cells were recovered immediately with warm media for 6 h. Guide sequences: AAVS1-sg1 5′ GGGGCCACUAGGGACAGGAU 3′, ARID1A-sg58 5′ CCUGUUGACCAUACCCGCUG 3′, ARID1A-sg60 5′ UGUGGCUGCUGCUGAUACGA 3′.

Assessment of targeted CRISPR gene editing: 4–7 days after editing, genomic DNA was extracted with QuickExtract DNA Extraction Solution (Lucigen) and ~500 bp regions flanking the cut site were amplified with Phusion Hot Start Flex 2X Master Mix (New England Biolabs) according to manufacturer's instructions. Sanger sequencing traces were analyzed by Inference of CRISPR Editing (ICE).

Pooled CRISPR screen in primary human T cells *in vivo*

Activated human T cells from two donors were transduced by lentivirus to express the NY-ESO specific TCR, in parallel to lentiviral transduction of a sgRNA library with 2 sgRNAs per target gene and 8 negative controls. 24 h after transduction, cells were electroporated with Cas9 Protein, as previously described (Shifrut et al., 2018). After electroporation, T cells were expanded in complete X-vivo 15 medium and split every two days, supplementing IL-2 at 50 U/ml. On Day 7, 2 NSG mice per donor were injected subcutaneously with 1 x 10^6 A375 cells, as previously described (Roth et al., 2020). 1 x 10^6 TCR-positive T cells were transferred to mice 7 days later via retro-orbital injection. Tumors and spleens were collected 7 days after T cell transfer and processed to single cell suspension, as described previously (Roth et al., 2020). T cells were sorted by CD45 staining and gDNA was extracted using commercial kits. Library preparation, next generation sequencing and analysis was performed as previously described (Shifrut et al., 2018). The guide abundance in the spleen and tumor of each mouse was used to calculate log fold change of each guide, and MAGeCK scores were calculated with default parameters.

Direct-capture perturb-seq

For Perturb-seq experiments, we used direct-capture Perturb-seq because it does not require a vector with a barcode sequence separate from the sgRNA, or other modifications to standard sgRNA vectors, and thus was immediately compatible with our retroviral reagents (Replogle et al., 2020). We adapted the 10x Chromium Next GEM Single Cell V(D)J Reagent Kits v1.1 5′ scRNA with Feature Barcoding reagents and protocol to be compatible with direct capture of sgRNAs in single cells. Our procedure is conceptually similar to that of Replogle et al. and the modifications to the 10X genomics protocol are summarized here. For Step 1, GEM Generation and Barcoding, 5 pmol of primer KP_bead_sgRNA_RT was spiked into the reaction, enabling capture of sgRNAs in droplets and then reverse transcription of sgRNAs. Step 3.2B, Supernatant Cleanup for Cell Surface Protein Library was performed to isolate the sgRNA library. Finally, 2 uL of the product of Step 3.2B was amplified and indexed using 3 rounds of PCR. The 250bp library was purified via agarose gel and sequenced together with the gene expression (GEX) library in 26x91 format, according to 10X protocol guidelines. For Perturb-seq replicate samples shown in Figure S7B, each replicate represents either an individual tumor or two tumors from the same mouse combined into one sample. Tumors from the same mouse were combined if the cell yield was well under 10X guidelines for targeted recovery of 10,000 cells per capture. If cell yield was well over the amount needed for recovery of 10,000 cells, in certain cases samples were split across multiple 10X captures to maximize cell yield. Samples split across multiple captures were computationally merged and not counted as separate replicates.

QUANTIFICATION AND STATISTICAL ANALYSIS

Analysis summary

Statistical analysis and all software used is detailed in the below sub-sections. Statistical details for experiments, including the statistical test used, the value of n, and what n represents, can be found in the figure legends. Statistical significance was determined as $p < 0.05$ (or FDR <0.05, where appropriate) unless otherwise specified.

ATAC-seq analysis

Fastq files were trimmed using fastp (Chen et al., 2018) and aligned to the mm10 genome using hisat2 (Kim et al., 2019). Reads were deduplicated and a bed file for each sample containing filtered, deduplicated ATAC-seq fragments was created. Peaks for each sample were called individually using MACS2 (Zhang et al., 2008) and then filtered into reproducible peaks based on peaks present in the majority of replicates for that sample. A union peak set for all samples was constructed by merging reproducible peaks for each sample into a set of high-confidence non-overlapping fixed width (500bp) peaks, which was used to create a peak by sample matrix used in downstream analysis. Differential peaks were determined using DESeq2 (Love et al., 2014). Principal component analysis was performed on the peak matrix by first normalizing using 'DESeq2::varianceStabilizingTransformation' and then 'stats::prcomp'. Genome track files were created by loading the fragments for each sample into R, and exporting bigwig files normalized by reads in transcription start sites using 'rtracklayer::export'. Coverage files were visualized using the Integrative Genomics Viewer. For analysis of previously published ATAC-seq data (Miller et al., 2019), fastq files were downloaded from accession GSE123236 and re-processed using our pipeline for consistency. Terminal and Progeintor T_{EX} ATAC-seq peaks were computed using DESeq2 with cutoffs of

Log_2 FC ≥ 1 and FDR ≤ 0.05 when comparing Terminal versus Progenitor T_{EX} samples (either TIL samples or LCMV samples, as indicated). For quantification of overlapping peaks between published data and *in vitro* assay data, a union peak set was created encompassing all samples and re-analyzed. For HOMER motif enrichment analysis shown in Figure S8G, the HOMER findMotifsGenome command line utility was used to identify motifs present in peaks in the indicated peak set relative to a background peak set. For the background peak set, we used the union peak set of the considered samples, and as a result the enriched motifs correspond to motifs enriched in the differential peak set relative to our samples in aggregate, rather than motifs enriched in human T cells relative to random genomic regions.

Bulk sgRNA screening data analysis

sgRNA sequencing data was analyzed using our previously published pipelines (Flynn et al., 2021). Briefly, fastq files were trimmed using 'fastp -f 10 –max_len1 = 50'. Trimmed reads were aligned to a custom fasta file of the relevant pool (either the genome wide pool or the mini-pool) which was constructed by taking the sgRNA variable sequences and flanking them with the adjacent sequences in the pMSCV vector backbone. Alignment was performed using hisat2 with the –no-spliced-alignment option. Bam files were imported into R and converted into counts per guide using 'Rsamtools::scanBam'. A table of guides per sample was constructed in R and normalized by multiplying each count by 1e6, dividing by the total counts in that sample, adding 1, and then log2 normalizing. Log fold changes between two conditions (chronic vs acute or tumor vs input) were computed and then z-scored by subtracting the reference LFC average and dividing by the reference LFC standard deviation. For genome-wide screens, all guides were used as the reference and for mini-pool screens the control guides were used as the reference. p-values were computed from z-scores using the normal distribution and then FDR was computed by correcting for multiple hypothesis testing using 'p.adjust' in R. For the Gini index analysis shown in Figure S2, the 'ineq' R package was used.

Comparison of CRISPR screen analytical methods

To validate our analysis strategy, we also analyzed the genome-wide screen results with two widely used methods, MAGeCK and casTLE, which showed a high correlation between effect size estimates (casTLE effect size correlation: R = 0.66; MAGeCK log fold change correlation: R = 0.77; Figures S3A–S3D, Table S2) (Li et al., 2014; Morgens et al., 2016). A comparison of the genes classified as hits using each method revealed that the largest group of hits were shared by all three methods (''hit'' corresponds to FDR <0.05 for our pipeline and MAGeCK or casTLE score >10; Figure S3B). Finally, we sought to ensure that the identification of screen hits was robust to the choice of reference sgRNAs. We compared our normalization strategy (relative to all sgRNAs in the pool) to a strategy that utilizes a set of sgRNAs targeting olfactory receptors that are not expressed or predicted to function in T cells (Gilbert et al., 2014). We found that normalizing sgRNA enrichments to the olfactory receptor sgRNA set modestly boosted the statistical power of the screen results but otherwise had a minimal impact on the results (Figure S3E).

GO term analysis

For gene categorizations shown in Figure 2B and elsewhere, gene sets were defined as: TCR - KEGG_T_CELL_RECEPTOR_SIGNALING_PATHWAY, Chromatin - GOCC_CHROMATIN, Integrin - GOBP_INTEGRIN_ACTIVATION, Inhibitory receptor - GOBP_NEGATIVE_REGULATION_OF_LYMPHOCYTE_ACTIVATION. Gene lists were manually supplemented with the following genes: Chromatin - *ZFP219*, *TBX21*, *KDM6A*, *ELMSAN1*, *DNTTIP1*, *SETD1B*, *TADA2B*, *ZFP217*, *EOMES*. Integrins - *ITGB3*, *APBB1IP*, *ITGAV*. Inhibitory receptors - *PDCD1*. For the gene set enrichment analysis shown in Figure 2D and elsewhere, the indicated gene list was uploaded to the online gProfiler tool (available at https://biit.cs.ut.ee/gprofiler/gost).

Cytoscape interaction network

100 top enriched genes and 20 top depleted genes were imported into Cytoscape (Shannon et al., 2003). Edges were created by using the stringApp Cytoscape plugin to import known protein-protein interactions curated from string-db (Szklarczyk et al., 2019). A cutoff of stringdb score ≥ 0.75 was used to filter these protein protein interactions, which represents a conservative cutoff for identifying only high confidence interactions. Nodes were grouped based on GO Term analysis, subcellular localization, and/or manual curation. A small number of poorly characterized and/or disconnected nodes were removed from the visualization.

Direct-capture perturb-seq analysis

Fastq files were processed using the 10X cellranger count pipeline with feature barcode analysis enabled to process the GEX library and sgRNA library together. The mm10 reference transcriptome was used for the GEX library. For the sgRNA library, a feature reference spreadsheet was constructed which contained the variable sequence of each guide (reverse complemented since it was sequenced as part of read 2), guide ID, and target gene. The filtered matrices for both 'Gene Expression' and 'CRISPR Guide Capture' were loaded into Seurat for downstream analysis (Hao et al., 2021). The Seurat 'IntegrateData' utility was used to merge the samples from the two independent experiments.

To assign sgRNAs to cells, we computed row z-scores for the 'CRISPR Guide Capture' matrix, quantifying how enriched each sgRNA was relative to other sgRNAs detected in the same cell. We also computed the difference in z-scores between the most-enriched and second-most enriched sgRNA. Cells which had a maximum sgRNA z-score ≥ 5 and a z-score difference ≥ 2 were determined to contain the guide with maximum z-score, while cells with no sgRNA counts were assigned as ''no guide,'' and other cells were assigned ''multi guide''. With this strategy, cells with multiple enriched sgRNAs due to retroviral infection doublets, single-cell capture doublets, and/or background reads were removed from further analysis. The guide assignments were added to the Seurat metadata for downstream processing. Seurat cell cycle scoring was used to predict the cell cycle phase of each single cell. All differential gene comparisons were performed using Seurat FindMarkers using the Wilcoxon test (the default statistical test). For volcano plot analysis, significantly differential genes were identified as FDR <0.05. For comparisons of different gene sets across perturbations, an addition fold change cutoff was applied of average $\log_2$ FC > 0.1 or average $\log_2$ FC < -0.1. For categorization of shared 'up' and 'down' gene sets within the cBAF and INO80 complexes (analysis shown in Figures 7D and 7E), the union set of significantly differential genes within each complex was aggregated, and then 'up' and 'down' genes for each subunit were defined simply as LFC >0 or LFC <0. This strategy was chosen to compare gene sets despite the different amounts of cells collected for each perturbation and resulting difference in statistical power to reach the FDR <0.05 threshold.

For comparisons to T cell signatures from acute and chronic LCMV infections (for example, in Figures 6E and 7G), we analyzed a previously described scRNA-seq dataset (Daniel et al., 2021). Briefly, the T_{EFF}, T_{MEM}, and T_{EM} clusters primarily contain T cells from the acute LCMV infection samples, and T_{EX}eeff, T_{EX}KLR, T_{EX}ISG, T_{EX}Term, T_{EX}Int, and T_{EX}Prog clusters primarily contain cells from the chronic LCMV infection samples. Clonal analysis supports a differentiation trajectory wherein early effector T_{EX} cells (T_{EX}eeff) give rise to T_{EX}Prog (progenitor exhausted) and T_{EX}Int (intermediate exhausted) subtypes. These cells differentiate into terminally exhausted cells (T_{EX}Term) or effector-like KLR-expressing exhausted cells (T_{EX}KLR). Seurat gene module scoring was used to convert the LCMV gene sets (consisting of the top 100 marker genes per LCMV cluster) into a gene module score for each cell in the Perturb-seq dataset. Gene module scoring was also used to convert the upregulated and downregulated gene sets into module scores for each cell in the expanded LCMV data set, as shown in Figure S8.

Cancer Cell, Volume *40*

Supplemental information

Genome-wide CRISPR screens of T cell exhaustion identify chromatin remodeling factors that limit T cell persistence

Julia A. Belk, Winnie Yao, Nghi Ly, Katherine A. Freitas, Yan-Ting Chen, Quanming Shi, Alfredo M. Valencia, Eric Shifrut, Nupura Kale, Kathryn E. Yost, Connor V. Duffy, Bence Daniel, Madeline A. Hwee, Zhuang Miao, Alan Ashworth, Crystal L. Mackall, Alexander Marson, Julia Carnevale, Santosh A. Vardhana, and Ansuman T. Satpathy

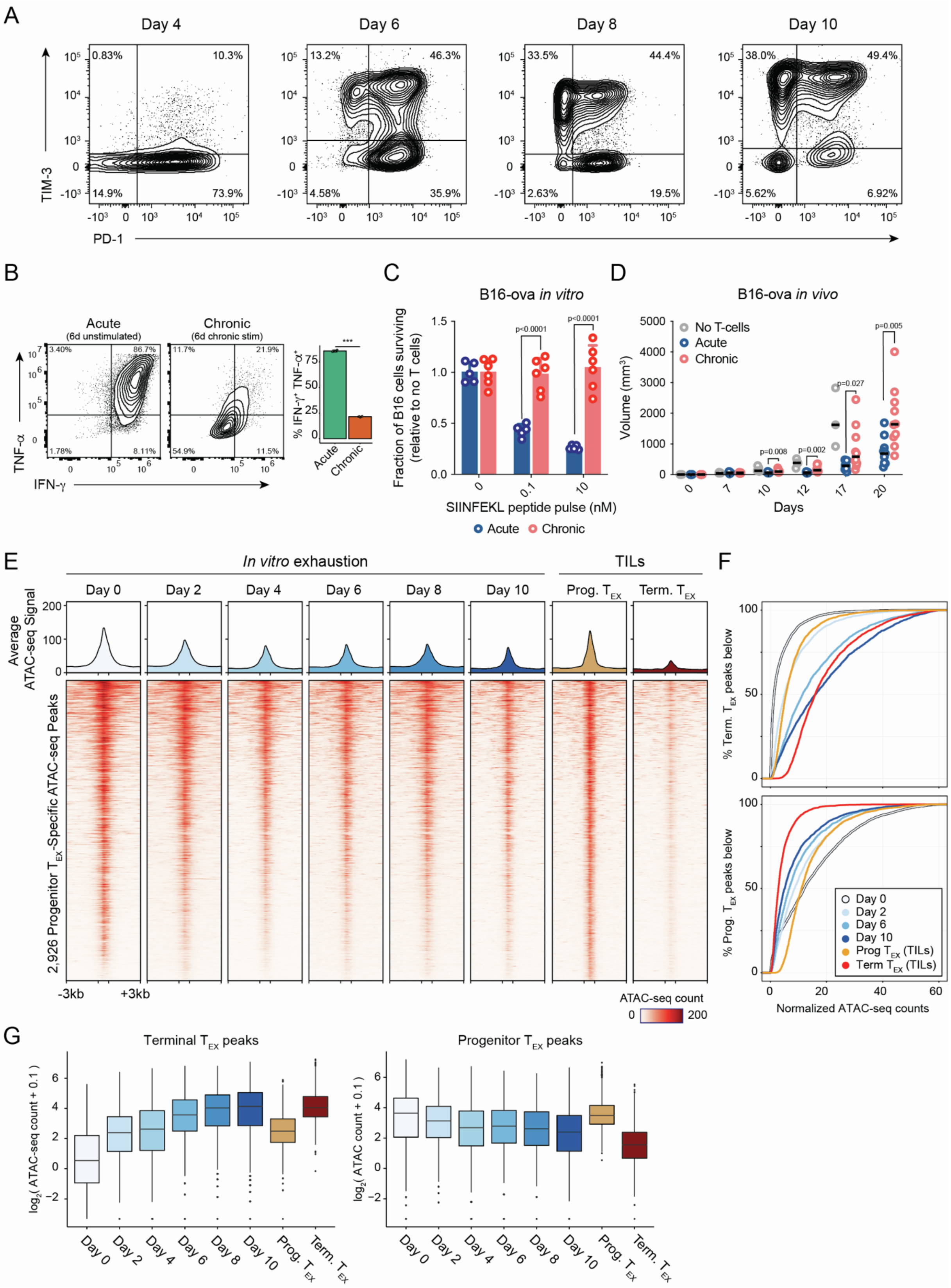

Figure S1. Additional characterization of *in vitro* assay, related to Figure 1. (A) Surface phenotype of chronically stimulated T cells throughout the *in vitro* exhaustion assay. **(B)** Effector cytokine production of acutely (left) and chronically (right) stimulated T cells after 6 days of chronic stimulation (day 8 after isolation), n=3. Cells were restimulated with PMA and ionomycin 8 days after initial stimulation. **(C)** Survival of B16 cells after co-culture with acutely or chronically stimulated OT-1 T cells, n=3 or n=4 as indicated. Tumor cells were pulsed with cognate peptide (SIINFEKL). **(D)** B16-ovalbumin tumor growth *in vivo* after adoptive transplant of acutely or chronically stimulated T cells, n=10 except for “No T-cells” (n=3). **(E)** Heatmap showing ATAC-seq coverage of each peak in the “Progenitor T_{EX} peak set” for each time point in the *in vitro* exhaustion assay. Reference data from TILs is also included. **(F)** Empirical cumulative distribution of peak accessibility for peaks in the Term. T_{EX} peak set (top) and Prog. T_{EX} peak set (bottom) for the indicated time points *in vitro*. Reference profiles from TILs are included as indicated. **(G)** Box plots for the indicated peak sets in the *in vitro* exhaustion assay and reference TIL samples, n=3,537 Terminal T_{EX} peaks or n=2,926 Progenitor T_{EX} peaks. Each dot represents one peak. Box plots show 25th, 50th (median), and 75th percentiles with outliers shown as dots. For **(E-G)**, one representative replicate is shown for each sample.

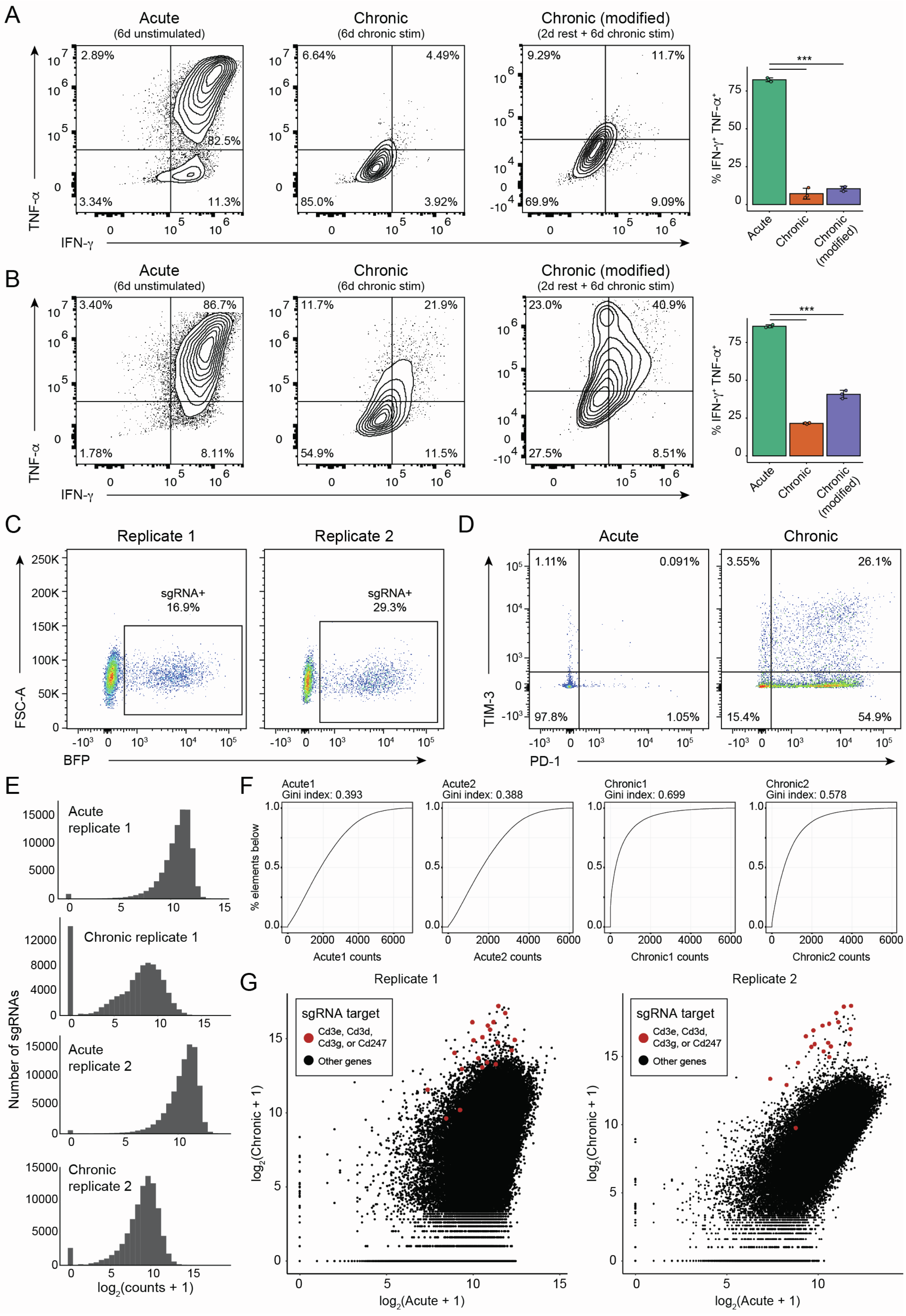
A
Acute
(6d unstimulated)
Chronic
(6d chronic stim)
Chronic (modified)
(2d rest + 6d chronic stim)
2.89%
82.5%
3.34%
11.3%
6.64%
4.49%
85.0%
3.92%
9.29%
11.7%
69.9%
9.09%
TNF-α
IFN-γ
% IFN-γ+ TNF-α+
***
Acute
Chronic
Chronic (modified)
B
Acute
(6d unstimulated)
Chronic
(6d chronic stim)
Chronic (modified)
(2d rest + 6d chronic stim)
3.40%
86.7%
1.78%
8.11%
11.7%
21.9%
54.9%
11.5%
23.0%
40.9%
27.5%
8.51%
TNF-α
IFN-γ
% IFN-γ+ TNF-α+
***
Acute
Chronic
Chronic (modified)
C
Replicate 1
Replicate 2
sgRNA+
16.9%
sgRNA+
29.3%
FSC-A
BFP
250K
200K
150K
100K
50K
D
Acute
Chronic
1.11%
0.091%
97.8%
1.05%
3.55%
26.1%
15.4%
54.9%
TIM-3
PD-1
E
Acute replicate 1
Chronic replicate 1
Acute replicate 2
Chronic replicate 2
Number of sgRNAs
log2(counts + 1)
F
Acute1
Gini index: 0.393
Acute2
Gini index: 0.388
Chronic1
Gini index: 0.699
Chronic2
Gini index: 0.578
% elements below
Acute1 counts
Acute2 counts
Chronic1 counts
Chronic2 counts
G
Replicate 1
Replicate 2
sgRNA target
Cd3e, Cd3d, Cd3g, or Cd247
Other genes
log2(Chronic + 1)
log2(Acute + 1)

Figure S2. Validation of assay modifications and quality control data for *in vitro* genome wide screen, related to Figure 2. (A-B) Comparison of cytokine production after acute stimulation, chronic stimulation (6 days of anti-CD3 stimulation), or the modified chronic stimulation protocol (6 days of anti-CD3 stimulation after a 48-hour rest). **(A)** Cytokine production after anti-CD3 re-stimulation, n=3. **(B)** Cytokine production after PMA re-stimulation, n=3. **(C)** Expression of BFP on day 2 of the screen. **(D)** Surface phenotype of cells before gDNA extraction. **(E)** sgRNA representation of each sample, n=2000 sgRNAs. **(F)** Gini index and empirical cumulative distribution function shown for each sample in the genome-wide screen. **(G)** sgRNA count correlations (Acute vs Chronic) for each replicate. CD3 subunits are shown in red, all other sgRNAs in black.

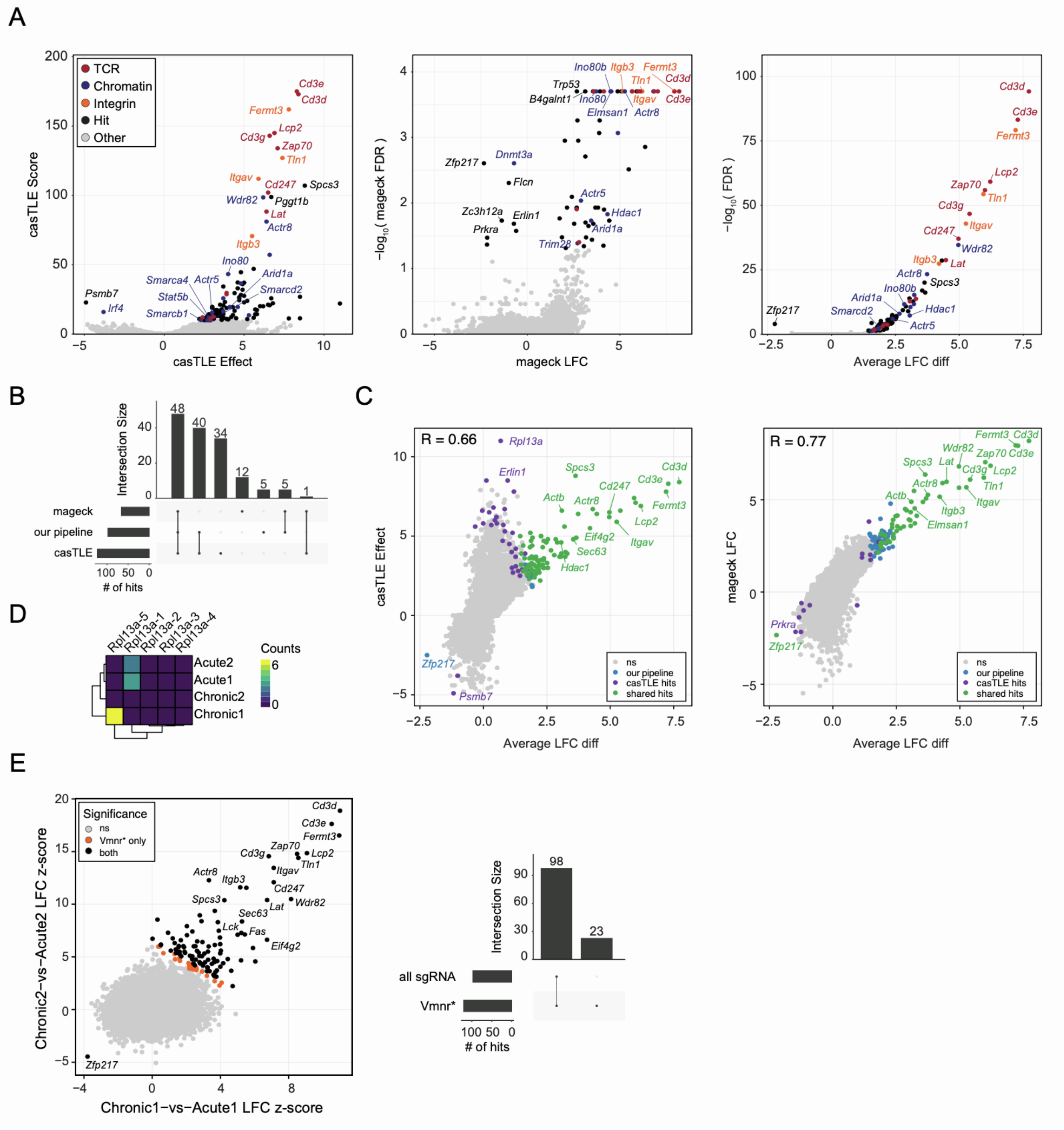

Figure S3. Comparison of CRISPR analysis strategies, related to Figure 2. (A) Volcano plots of genome wide CRISPR screen results using casTLE (left), MAGeCK (center), and our pipeline (right). **(B)** Comparison of hit lists for each of the three pipelines. **(C)** Comparison of LFC difference computed by our pipeline to the casTLE Effect (left) and MAGeCK LFC (right). **(D)** Counts table shown for *Rpl13a*. **(E)** Genome wide screen results when z-scores are computed relative to all sgRNAs or a set of olfactory receptors (Vmnr* genes).

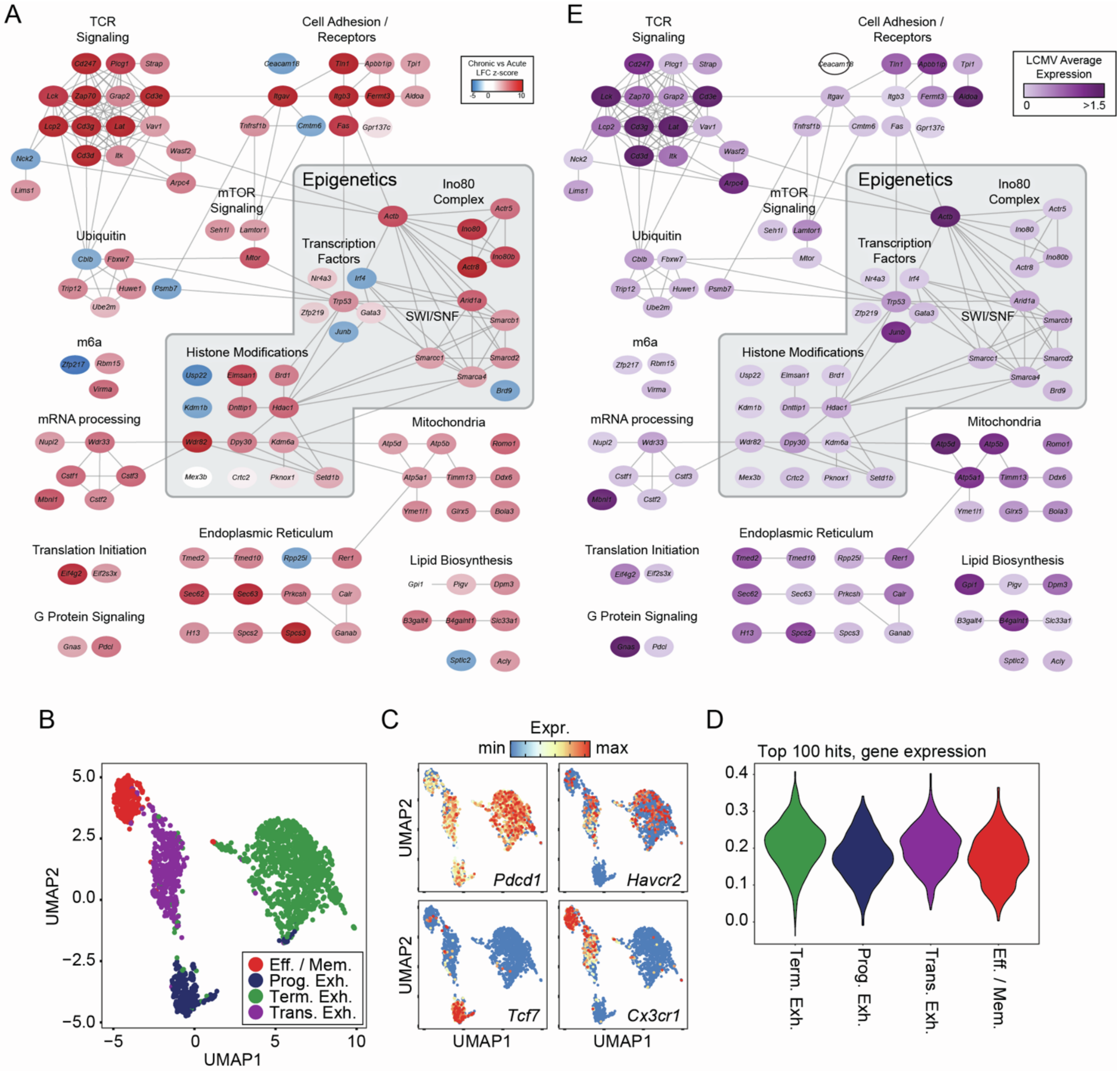

Figure S4. Cytoscape network representation of top hits and LCMV clone 13 expression analysis, related to Figure 2. (A) Top positive and negative hits from the genome-wide screen are shown. Each protein is represented by a node in the cytoscape network, colored by its z-score in the genome-wide screen. Nodes are connected if there is a high confidence protein-protein interaction in the string-db database (Szklarczyk et al., 2019). **(B)** Cell types identified in previously published scRNA-seq data (Raju et al., 2021). **(C)** Expression of *Pdcd1*, *Havcr2*, *Tcf7*, and *Cx3cr1* in single cells. **(D)** Expression of the gene module containing the top 100 *in vitro* hits across clusters. **(E)** Cytoscape network of top hits colored by average expression across all single cells.

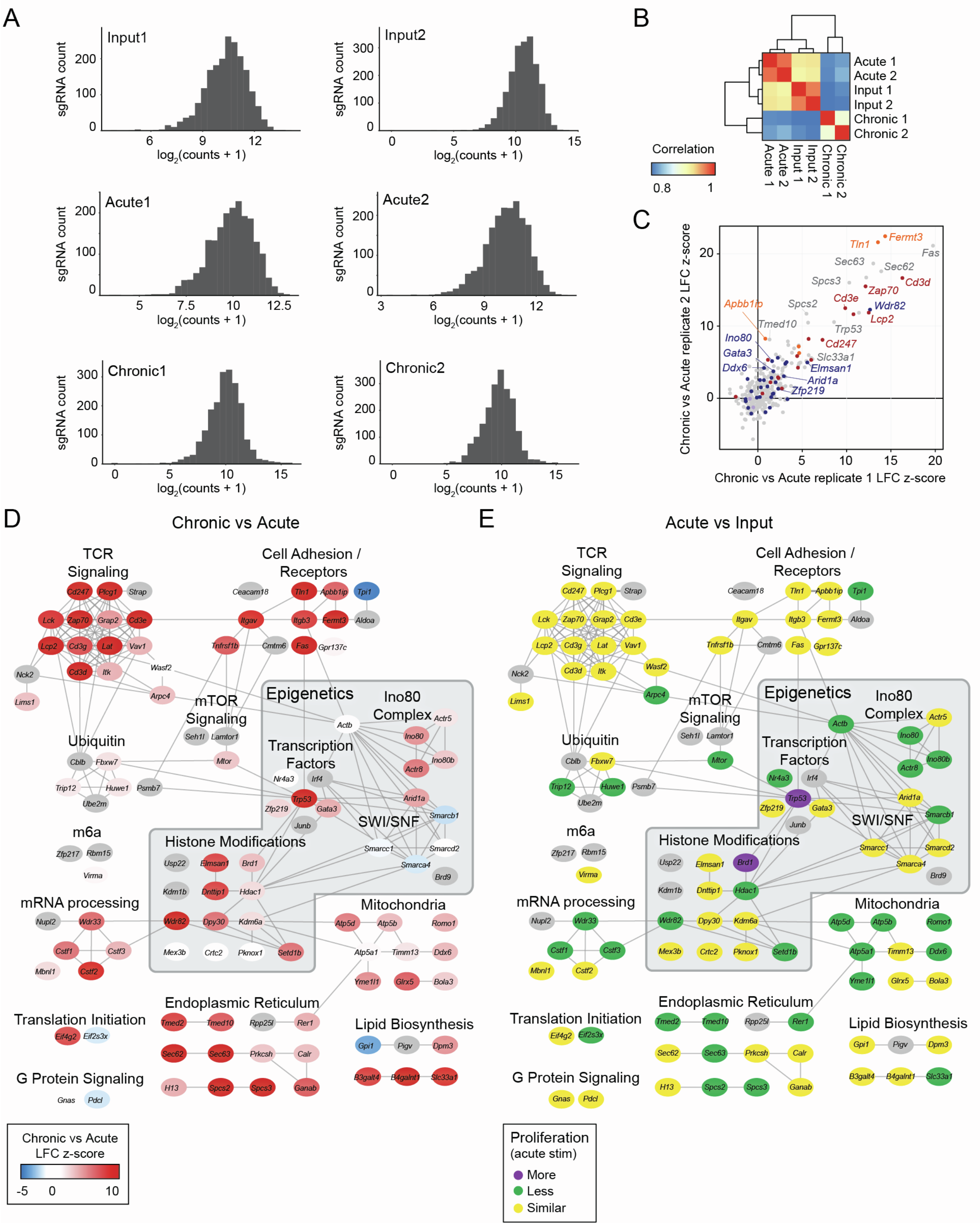

Figure S5. Additional data for targeted *in vitro* screening, related to Figure 2. (A) sgRNA representation of each sample in the *in vitro* mini-pool screen. **(B)** Correlation of the sgRNA counts of each sample in the mini-pool screen. **(C)** Correlation of the Chronic vs Acute replicate z-scores, n=2. **(D)**

Cytoscape interaction network with genes colored by their z-score in the Chronic vs Acute mini-pool screen. **(E)** Cytoscape interaction network with genes colored by their fitness categorization in acute stimulation.

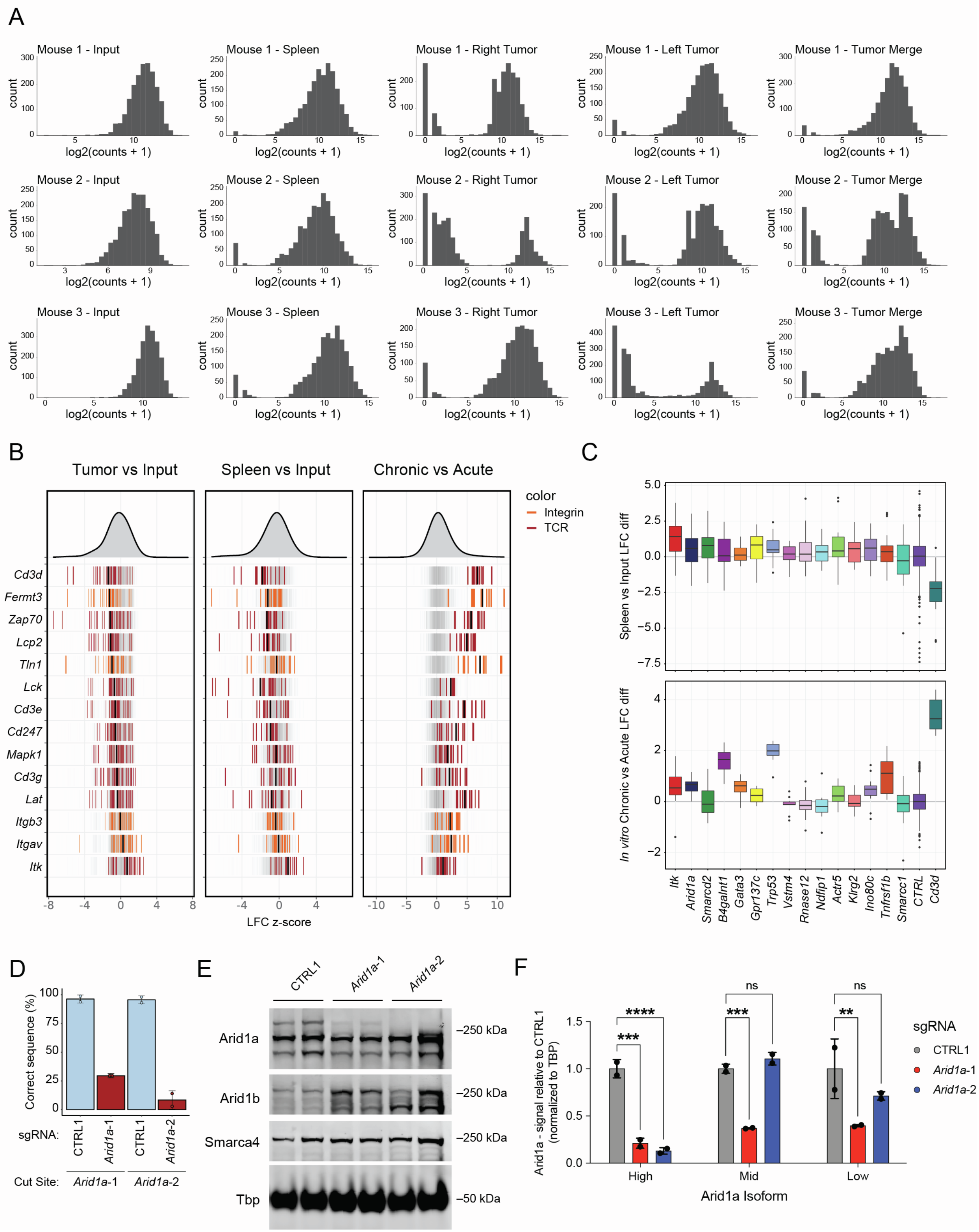

Figure S6. Additional data for targeted *in vivo* screening and validation of *Arid1a*-targeting sgRNAs, related to Figures 3 and 4. (A) sgRNA pool coverage for each sample in the *in vivo* mini-pool screen. **(B)** sgRNA z-scores in MC-38 tumors (n=36 sgRNA-replicates), MC-38 spleens (n=18 sgRNA-replicates), and *in vitro* mini-pool Chronic vs Acute (n=12 sgRNA-replicates) for selected genes in the “TCR signaling” and “Integrin signaling” categories. **(C)** Boxplot of spleen vs input (n=18 except for CTRL (n=600)) and acute vs chronic (n=12 except for CTRL (n=400)) log fold change for each sgRNA targeting the indicated gene, with the mean control log fold change subtracted. Box plots show 25th, 50th (median), and 75th percentiles with outliers shown as dots. **(D)** Sanger sequencing (TIDE) analysis of editing efficiency of *Arid1a* sgRNAs, n=2 replicates per sgRNA. Error bars denote mean ± SD. **(E)** Western blot analysis of protein knockdown for Arid1a sgRNAs, as well as Arid1b and Smarca4 expression. **(F)** Quantification of protein knockdown for each identified isoform of *Arid1a* (panel C three bands), n=2. * $p < 0.05$, ** $p < 0.01$, *** $p < 0.001$, **** $p < 0.0001$.

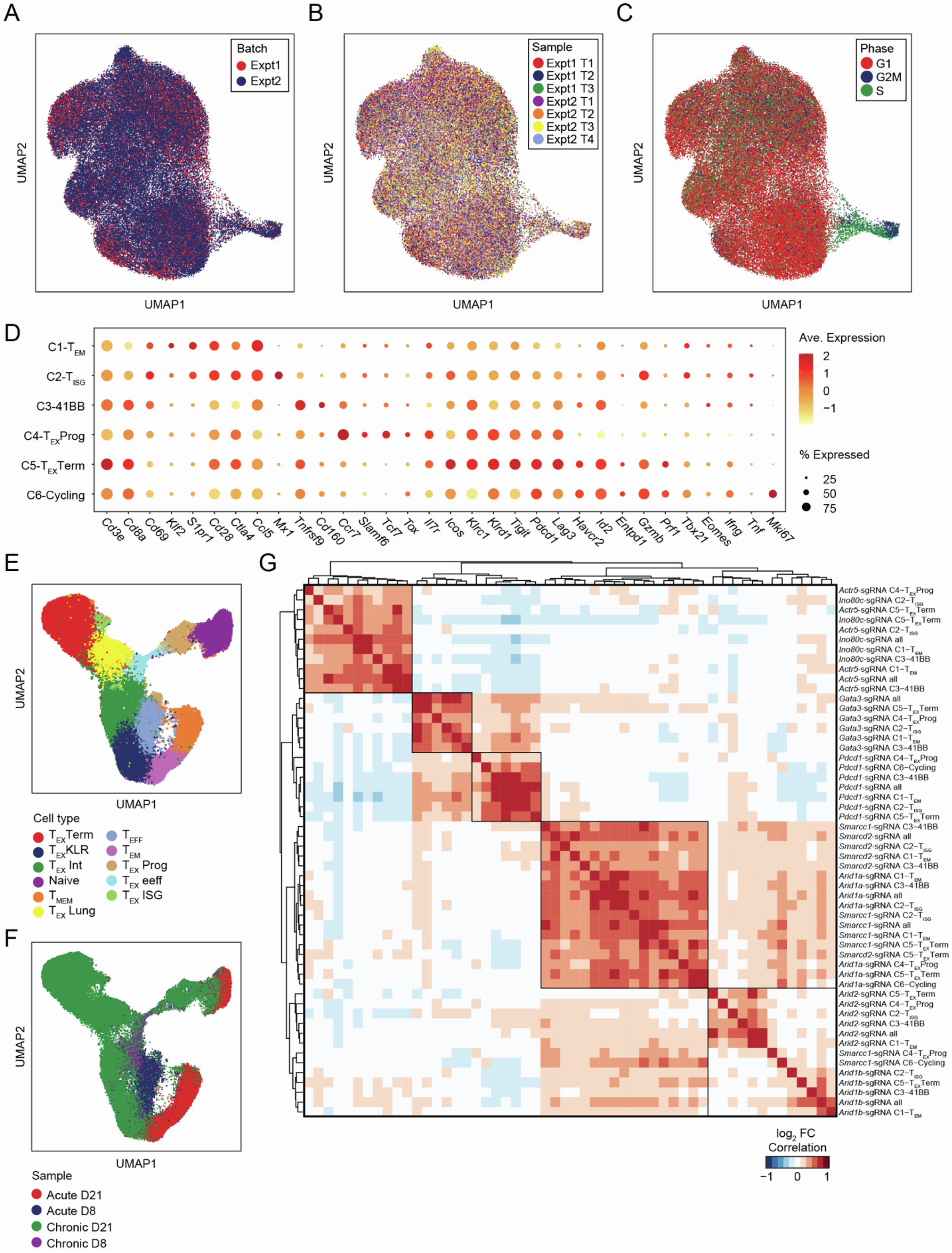
A
Batch
Expt1
Expt2
UMAP2
UMAP1
B
Sample
Expt1 T1
Expt1 T2
Expt1 T3
Expt2 T1
Expt2 T2
Expt2 T3
Expt2 T4
UMAP2
UMAP1
C
Phase
G1
G2M
S
UMAP2
UMAP1
D
C1-T_EM
C2-T_ISG
C3-41BB
C4-T_EX Prog
C5-T_EX Term
C6-Cycling
Cd3e Cd8a Cd69 Klf2 S1pr1 Cd28 Ctla4 Ccl5 Mx1 Tnfrsf9 Cd160 Ccr7 Slamf6 Tcf7 Tox Il7r Icos Klrc1 Klrd1 Tigit Pdcd1 Lag3 Havcr2 Id2 Entpd1 Gzmb Prf1 Tbx21 Eomes Ifng Tnf Mki67
Ave. Expression
2
1
0
−1
% Expressed
25
50
75
E
UMAP2
UMAP1
Cell type
T_EX Term
T_EX KLR
T_EX Int
Naive
T_MEM
T_EX Lung
T_EFF
T_EM
T_EX Prog
T_EX eeff
T_EX ISG
F
UMAP2
UMAP1
Sample
Acute D21
Acute D8
Chronic D21
Chronic D8
G
Actr5-sgRNA C4−T_EX Prog
Ino80c-sgRNA C2−T_ISG
Actr5-sgRNA C5−T_EX Term
Ino80c-sgRNA C5−T_EX Term
Actr5-sgRNA C2−T_ISG
Ino80c-sgRNA all
Ino80c-sgRNA C1−T_EM
Ino80c-sgRNA C3−41BB
Actr5-sgRNA C1−T_EM
Actr5-sgRNA all
Actr5-sgRNA C3−41BB
Gata3-sgRNA all
Gata3-sgRNA C5−T_EX Term
Gata3-sgRNA C4−T_EX Prog
Gata3-sgRNA C2−T_ISG
Gata3-sgRNA C1−T_EM
Gata3-sgRNA C3−41BB
Pdcd1-sgRNA C4−T_EX Prog
Pdcd1-sgRNA C6−Cycling
Pdcd1-sgRNA C3−41BB
Pdcd1-sgRNA all
Pdcd1-sgRNA C1−T_EM
Pdcd1-sgRNA C2−T_ISG
Pdcd1-sgRNA C5−T_EX Term
Smarcc1-sgRNA C3−41BB
Smarcd2-sgRNA all
Smarcd2-sgRNA C2−T_ISG
Smarcd2-sgRNA C1−T_EM
Smarcd2-sgRNA C3−41BB
Arid1a-sgRNA C1−T_EM
Arid1a-sgRNA C3−41BB
Arid1a-sgRNA all
Arid1a-sgRNA C2−T_ISG
Smarcc1-sgRNA C2−T_ISG
Smarcc1-sgRNA all
Smarcc1-sgRNA C1−T_EM
Smarcc1-sgRNA C5−T_EX Term
Smarcd2-sgRNA C5−T_EX Term
Arid1a-sgRNA C4−T_EX Prog
Arid1a-sgRNA C5−T_EX Term
Arid1a-sgRNA C6−Cycling
Arid2-sgRNA C5−T_EX Term
Arid2-sgRNA C4−T_EX Prog
Arid2-sgRNA C2−T_ISG
Arid2-sgRNA C3−41BB
Arid2-sgRNA all
Arid2-sgRNA C1−T_EM
Smarcc1-sgRNA C4−T_EX Prog
Smarcc1-sgRNA C6−Cycling
Arid1b-sgRNA C2−T_ISG
Arid1b-sgRNA C5−T_EX Term
Arid1b-sgRNA C3−41BB
Arid1b-sgRNA all
Arid1b-sgRNA C1−T_EM
log2 FC
Correlation
−1
0
1

Figure S7. Additional data on the *in vivo* Perturb-seq experiment, related to Figure 6. (A) scRNA-seq profiles of TILs colored by each independent experiment (n=2 independent experiments). **(B)** scRNA-seq profiles of TILs colored by each sample (n=7 replicates). **(C)** scRNA-seq profiles of TILs colored by predicted phase of the cell cycle. **(D)** Additional marker genes shown for each cluster. **(E)** Expanded reference LCMV dataset with single cell profiles colored by LCMV cluster. Data from (Daniel et al., 2021). **(F)** Expanded LCMV dataset with single cell profiles colored by LCMV infection (Acute corresponds to Armstrong infection while Chronic corresponds to Clone 13) and time point (Day 8 or Day 21 post infection). **(G)** Heatmap of the correlation of gene expression differences subsetted on each cluster. The indicated gene knockdown was compared to CTRL1 cells within each cluster. Comparisons with <150 cells in the comparison groups are excluded due to lack of statistical power.

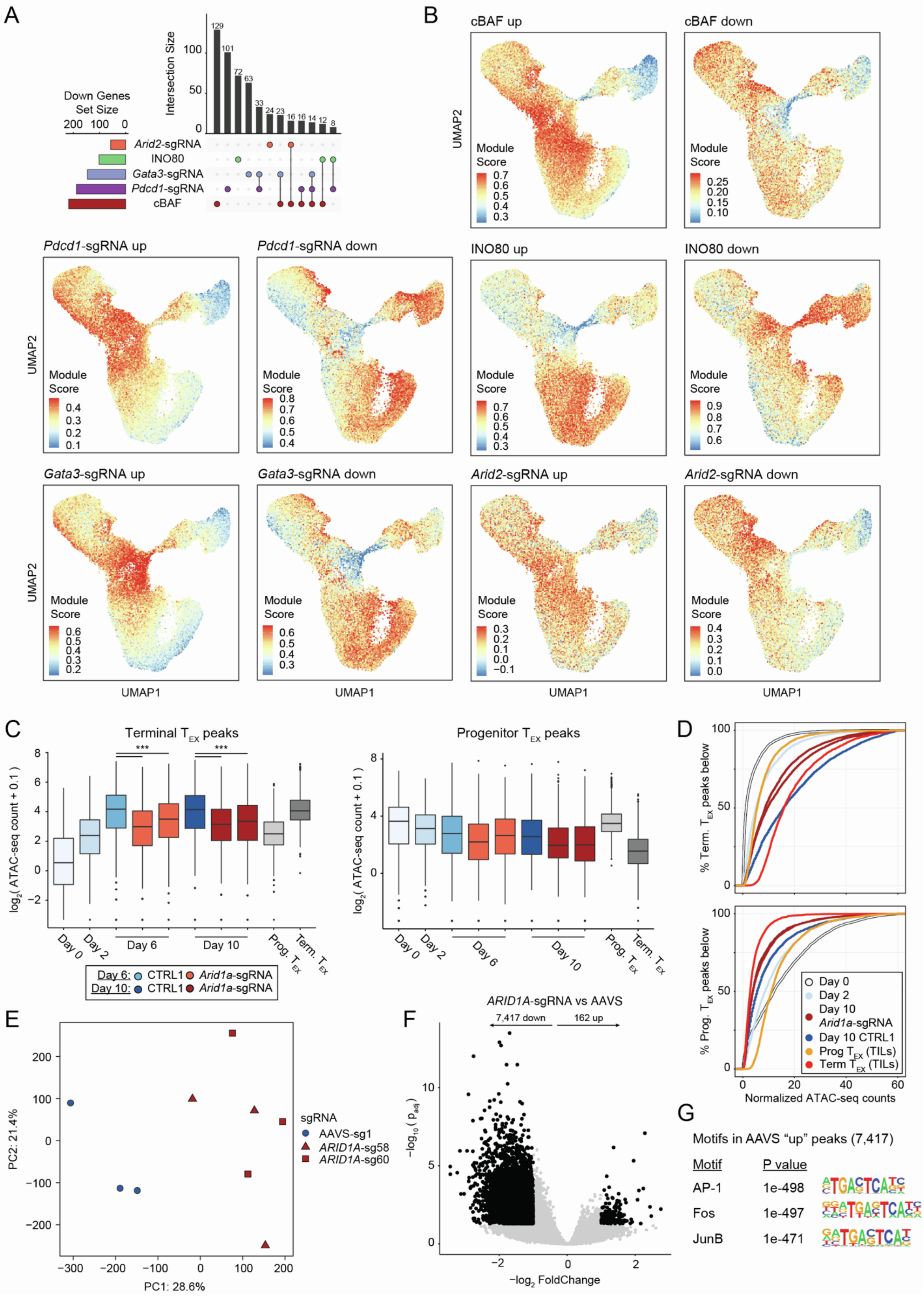
A
Down Genes
Set Size
200 100 0
Intersection Size
129 101 72 63 33 24 23 16 16 14 12 8
Arid2-sgRNA
INO80
Gata3-sgRNA
Pdcd1-sgRNA
cBAF
B
cBAF up
cBAF down
Pdcd1-sgRNA up
Pdcd1-sgRNA down
INO80 up
INO80 down
Gata3-sgRNA up
Gata3-sgRNA down
Arid2-sgRNA up
Arid2-sgRNA down
Module Score
UMAP1
UMAP2
C
Terminal T$_{EX}$ peaks
Progenitor T$_{EX}$ peaks
log$_2$(ATAC-seq count + 0.1)
***
Day 0
Day 2
Day 6
Day 10
Prog. T$_{EX}$
Term. T$_{EX}$
Day 6: CTRL1 Arid1a-sgRNA
Day 10: CTRL1 Arid1a-sgRNA
D
% Term. T$_{EX}$ peaks below
% Prog. T$_{EX}$ peaks below
Normalized ATAC-seq counts
Day 0
Day 2
Day 10 Arid1a-sgRNA
Day 10 CTRL1
Prog T$_{EX}$ (TILs)
Term T$_{EX}$ (TILs)
E
PC1: 28.6%
PC2: 21.4%
sgRNA
AAVS-sg1
ARID1A-sg58
ARID1A-sg60
F
ARID1A-sgRNA vs AAVS
7,417 down
162 up
−log$_{10}$ (p$_{adj}$)
−log$_2$ FoldChange
G
Motifs in AAVS "up" peaks (7,417)
Motif
P value
AP-1 1e-498
Fos 1e-497
JunB 1e-471

Figure S8. Additional data on up- and downregulated gene sets and additional ATAC-seq data, related to Figures 7 and 8. (A) Comparison of gene sets downregulated by perturbation of cBAF subunits, INO80 subunits, or *Pdcd1*-sgRNA, *Gata3*-sgRNA, or *Arid2*-sgRNA. **(B)** Module scores of the indicated gene sets computed for each cell in the expanded LCMV reference dataset. **(C)** Box plots for the indicated peak sets in the *in vitro* exhaustion assay and reference TIL samples. Each dot represents one peak, n=3,537 Terminal T_{EX} peaks or n=2,926 Progenitor T_{EX} peaks**.** Box plots show 25th, 50th (median), and 75th percentiles with outliers shown as dots. Significance determined by Wilcoxon test, *** $p < 0.001$. **(D)** Empirical cumulative distribution of peak accessibility for peaks in the Term. T_{EX} peak set (top) and Prog. T_{EX} peak set (bottom) for the indicated samples *in vitro*. Reference profiles from TILs are included as indicated. **(E)** Principal component analysis of ATAC-seq data of primary human T cells chronically stimulated for six days, n=3 per sgRNA. **(F)** Differential peaks between *ARID1A*-sgRNA and AAVS primary human T cells. **(G)** HOMER analysis of TF motifs enriched in AAVS ‘up’ peaks. Selected highly ranked motifs are shown. Results in **(E-G)** are merged from three different human donors in two independent experiments with two different *ARID1A* targeting sgRNAs per donor.